



UNICA

UNIVERSITÀ
DEGLI STUDI
DI CAGLIARI



Università di Cagliari

UNICA IRIS Institutional Research Information System

This is the Author's manuscript version of the following contribution:

V. L. Kotov , A. M. Bragov , V. V. Balandin, L. A. Igumnov , A. K. Lomunov, V. A. Eremeyev, A. Cazzani, "Cavity-expansion approximation for projectile impact and penetration into sand", *Continuum Mechanics and Thermodynamics*, **34**(2), 2022, pp. 395–421.

The publisher's version is available at:

<http://dx.doi.org/10.1007/s00161-021-01062-8>

When citing, please refer to the published version.

1 **Cavity-expansion approximation for projectile impact and penetration into sand**

2
3 V.L. Kotov¹, A.M. Bragov¹, V.V. Balandin¹, L.A. Igumnov¹, A.K. Lomunov¹, V.A. Eremeyev^{1,2},
4 A. Cazzani³

5
6 ¹*Research Institute of Mechanics, National Research Lobachevski State University of Nizhny*
7 *Novgorod, 23 Prospekt Gagarina (Gagarin Ave.), Building 6, GSP-1000, 603950, Nizhny*
8 *Novgorod, Russian Federation*

9 ²*Gdansk University of Technology, ul Narutowica, 11/12, 80-233, Gdansk, Poland*

10 ³*University of Cagliari, DICAAR, 2, via Marengo, I-09123 Cagliari, Italy*

11
12 E-mail: vkotov@inbox.ru, bragov@mech.unn.ru, igumnov@mech.unn.ru,
13 eremeyev.victor@gmail.com, antonio.cazzani@unica.it

14
15
16 Corresponding author: L.A. Igumnov, National Research Lobachevski State University of
17 Nizhny Novgorod, 23 Prospekt Gagarina (Gagarin Ave.), Building 6, 603950, Nizhny
18 Novgorod, Russian Federation

19 E-mail: igumnov@mech.unn.ru

20
21
22 **Acknowledgements.** The authors are grateful to V.I. Balandin and E.Yu. Linnik for assistance
23 in the preparation of the article.

24

25

1 **Abstract:**

2 The shock adiabats for dry and wet sand were obtained in our plane-wave shock
3 experiments and earlier in the inverse impact experiment technique by using a measure bar with
4 a flat end. A one-dimensional problem of a spherical cavity expanding at a constant velocity
5 from a point in an infinite soil medium, which has a first-kind self-similar solution is considered.
6 Elastic-plastic deformation of the soil is described in a barotropic approximation, using a shock
7 adiabat and Mohr-Coulomb-Tresca limit yield criterion. The medium is assumed to be
8 incompressible behind the shock wave front propagating through the unperturbed medium. The
9 problem in this formulation was solved analytically. Besides, a generalized solution of the
10 problem was obtained numerically, which involves transition of a continuous elastic-plastic
11 wave into a plastic shock wave when pressure grows with the cavity expansion velocity.
12 Comparison of the analytical and numerical solutions shows that a linearized analytical solution
13 is a good approximation of the pressure along the boundary of the cavity as a function of its
14 expansion, except for low velocities. A formula for determining minimal pressure required for
15 the nucleation of a cavity has been obtained, accounting for internal friction, in the framework of
16 Mohr-Coulomb yield criterion, which generalizes a known solution for an ideally plastic medium
17 with Tresca yield criterion. Lower and upper bounds for the ratio of the discontinuity surface
18 velocity (the elastic-plastic interface) to the cavity expansion velocity have been obtained. The
19 linearized solution can be used for analyzing resistance to a rigid sphere penetrating into the soil.
20 The computational results are compared with known experimental relations for resistance to
21 spherical projectiles penetrating dry and water-saturated sand. Good agreement between the
22 numerical and experimental results is obtained without introducing any correcting coefficients.

23

24 **Key words:** shock adiabat; impact; spherical projectile; sand; cavity expansion;

25

26

1 **1. Introduction**

2
3 The expanding cavity problem is a classical problem of mechanics of deformable solids.
4 There exist many formulations of this problem differing in: a) the way compressibility of the
5 material is accounted for – linearly compressible media [1], incompressible media or media with
6 limited ultimate strain [2, 3]; b) the assumed yield criterion – Tresca [1, 4], Mohr-Coulomb [2],
7 Mohr-Coulomb with Tresca-limit [3]. There is a solution of the problem obtained using Drucker-
8 Prager’s model and the non-associated yield law [5]. For brittle media (ice, ceramics, concrete),
9 the notion of the material failure zone is introduced [1, 6]. There also exists an improved
10 formulation of the problem, based on accounting for the dependence of the material properties on
11 strain rate [7, 8].

12 Papers [9 – 11] give approximations of cavity wall pressure as a function of its expansion
13 taking into account the induced variation of mechanical properties of the material as well as
14 parametric analysis of the obtained solutions. Alongside with dynamic formulations, static
15 formulations of the problem are also considered [12], which are especially popular in soil
16 mechanics [13 – 15]. Analytical solutions have been obtained for an incompressible elastic-
17 plastic medium, using different types of yield criterion; for compressible media, some effective
18 numerical algorithms [1] was proposed, based on the iterative method of numerical analysis of a
19 boundary-value problem for a system of two first-order ordinary differential equations, which
20 makes it possible to obtain an exact solution of the problem for the equation of state of a medium
21 with nonlinear relations [16, 17].

22 The expanding cavity problem has numerous applications in impact dynamics. The
23 approximate approach, in which pressure at every point of the lateral surface of the projectile is
24 identified with the pressure at the internal surface of a spherical cavity expanding in an infinite
25 medium from zero radius – the Cavity Expansion Method (CEM), is extensively used in
26 analyzing problems of impact and penetration into continua [18 – 22]. Analytic solutions of the

1 problem of a spherical cavity expanding in an incompressible elastic-plastic medium [4, 23 – 25]
2 using CEM are used in evaluating resistance forces and depths of penetration of rigid and
3 deformable strikers into metals, concrete and soils. It was noticed [25] that accounting for
4 incompressibility in metals at impact velocities up to 1 km/s produces insignificant effects. This
5 problem is still of scientific interest, as it is manifest in discussions [26 – 28] and [29 – 31].

6 The application of the approach based on solving the cavity expansion problem in the
7 dynamics of geological materials is presented in [1 – 3, 32, 33]. Along with these works, an
8 analysis of penetration of rigid and deformable projectiles at an angle to the free surface of a soil
9 medium, involving curvilinear motion trajectories, [34, 35] can be noticed. An experimental-
10 computational analysis of projectiles with flat, conical and hemispherical heads penetrating dry
11 and water-saturated sand is presented in [36 – 41].

12 Generally, it can be noticed that the analysis of the cavity expansion problem and the
13 methods of evaluating loads acting on the penetrator are well developed. Accounting for
14 nonlinear material properties, when analyzing problems of penetration into compressible elastic-
15 plastic media, poses no problem in numerically analyzing the cavity problem either.

16 One special feature in the deformation of soft soils is the necessity to account for both
17 continuous elastic-plastic and shock waves. The presence of spherical shock waves in sandy and
18 clayey soils, as well as the dependence of the shock wave velocity on the pressure at its front,
19 were shown experimentally [42 – 46]. It has to be noticed that the existing solutions of the cavity
20 expansion problem do not account for the possible formation of a shock wave propagating
21 through the unperturbed space.

22 The present article describes a formulation and analysis of a spherical cavity expansion
23 problem, which can be applied for evaluating the force resisting a rigid penetrator in sandy soil.
24 The deformational and shear properties of soil are assigned by a shock adiabat and Mohr-
25 Coulomb's with Tresca-limit yield criterion. The numerically obtained generalized solution
26 assumes the existence of an elastic region at subsonic propagation velocities of the elastic-plastic

1 interface and the formation of a single plastic shock wave at supersonic velocities. In the
2 assumption of incompressibility of the medium behind the shock wave front, an analytical
3 solution of the problem has been obtained. This solution is similar to the earlier obtained rigid-
4 plastic solution [1] of the cylindrical cavity expansion problem, where it was shown that use of a
5 rigid-plastic solution theoretically leads to overestimation of resistance to penetration. It should
6 be noticed, however, that the approach itself, based on using the analysis of the cavity expansion
7 problem in impact dynamics, is approximate; a solution is considered preferable, judging by its
8 results in comparison with the experimental data. By comparing the experimental and numerical
9 data, the present authors have demonstrated that the model of a rigid penetrator in soil, using a
10 simple linearized analytical rigid-plastic model, has a scope of applicability which is comparable
11 with models based on numerically analyzing the cavity expansion problem.

12

13 **2. Experimental methods of determining physical-mechanical properties of sand under** 14 **shockwave loading**

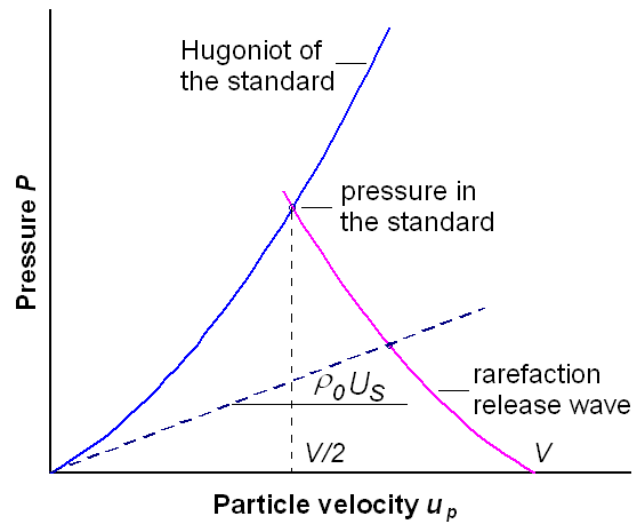
15

16 **2.1. The method of constructing a shock adiabat**

17

18 To study the dynamic compressibility of sand, the reflection method [47], also called the
19 impedance match technique, is used. In the method, the accelerated striker-plate hits a specimen
20 not directly, but through a screening plate. The shock adiabats of the materials of the striker and
21 the screen must be known. Besides, the initial density of the studied material must be determined
22 in advance. The measured parameters are shockwave front velocity U_s and striker velocity V ,
23 which (for equal properties of the striker and of the target) is equal to the double of particle mass
24 velocity u_p in the target (Fig. 1). These parameters in the shock wave are related through the
25 pulse conservation laws with the thermal-dynamic characteristics – pressure $P = \rho_0 U_s u_p$ and
26 impact compression density $\rho_s = \rho_0 U_s / (U_s - u_p)$. Measuring the two independent parameters
27 (namely U_s and u_p) makes it possible to determine the shock adiabat of the soil.

1



2

3

4

5

Fig. 1. A scheme for determining the shock adiabat of sand by using the impedance match technique.

6

7

8

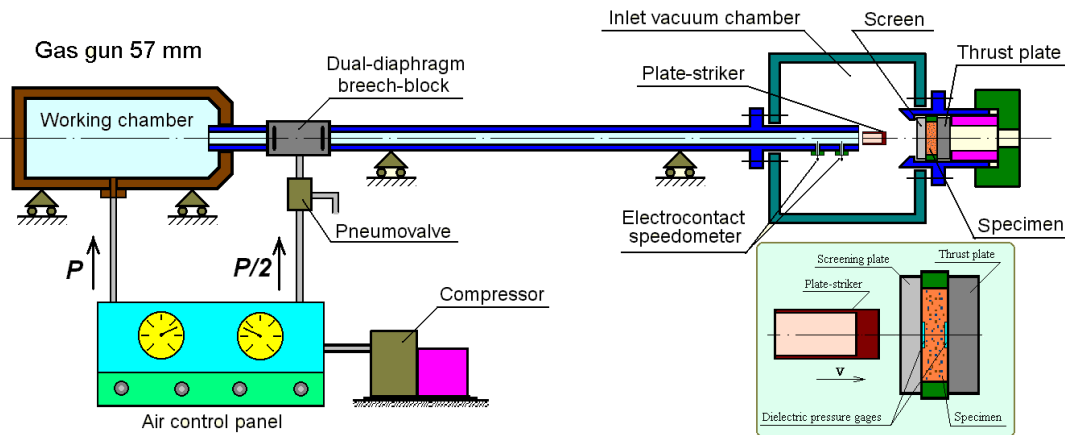
9

10

11

12

Fig.2 shows schematically an experimental stand used for realizing the methodology of constructing a shock adiabat using the reflection method. An 8mm-thick soil layer was placed between two plates made of an aluminum alloy. Compression waves were induced in a 5mm-thick screening plate struck by a projectile (impactor) which has been accelerated using a 57mm-caliber gas gun. As a result, a plane compression wave was formed both in the screening plate and in the specimen. The impact velocity varied in the range 100-500 m/s and was measured using electro-contact speedometers with an accuracy of up to 2%.



13

14

Fig. 2. The experimental stand (schematically).

1

2 The thicknesses of the plate-striker, of the screening plate and of the specimen were
3 chosen such that unloading waves from the free surfaces could not distort the picture of one-
4 dimensional strain in the compression wave. Changing impact velocity V and propagation
5 velocity U_s of the compression wave through the specimen in combination with known adiabats
6 of the striker and the screening plate makes it possible to determine the point of the shock
7 adiabat of the studied medium.

8 A 57mm-caliber gas gun was used to apply the loading. The propagation velocity of the
9 compressive wave in the specimen was measured with two dielectric pressure gauges located on
10 the specimen surfaces. Each gauge consisted of two 0.05mm-thick 20mm-diameter current
11 collectors made of copper foil and a 0.05mm-thick sensitive element of dielectric (PET film).
12 The total thickness of the gauge is 0.2 mm. When a plane wave travels through the specimen
13 within the gauges, the compression pulse induces electric signals on the armature of the gauges,
14 which are registered in the memory of the oscillograph. The compression wave propagation
15 velocity through the soil specimen can be determined based on the distance between the gauges
16 and the travelling time of the pressure pulses relative to each other. In testing soil materials in
17 conditions of shockwave loading, special attention was paid to inducing a plane wave with one-
18 dimensional strain. Inducing a plane wave is possible provided that warping is minimized, when
19 the striker hits the screening plate. Accordingly, the parallelism of the planes of the specimen
20 and the striker was thoroughly checked before each test.

21 To synchronize the time base of the oscillograph with the beginning of the process, an
22 electro-contact gauge, in the form of a 0.05mm-thick copper foil stripe cemented on a 0.05mm-
23 thick insulating film, was secured on the surface of the screening plate impacted by the plate-
24 striker. When the projectile hit the plate, the gauge short-circuited and triggered the oscillograph
25 to start recording.

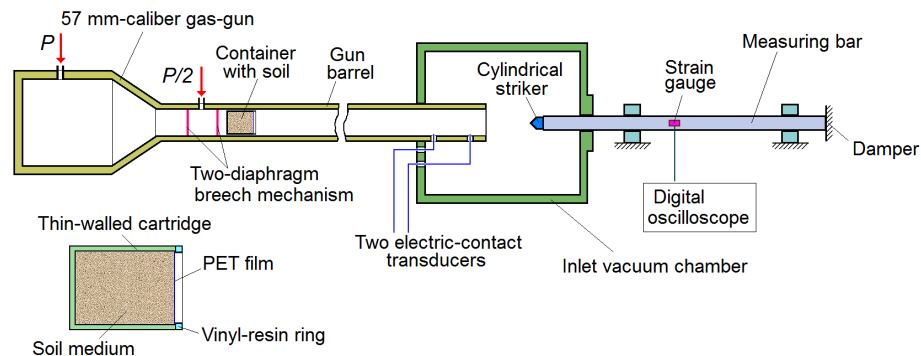
1 The analysis of the measurements and of processing the test data in the plane-wave
2 experiments showed that the inaccuracies in determining the parameters of shock adiabats are
3 less than 7% [48].

4 Experimenting with different impact velocities makes it possible to obtain several points
5 of the shock adiabat of the material.

6

7 **2.2. The inverse experiment technique using the measuring bar**

8 The methodology of measuring the force resisting penetration of a projectile into sand
9 using a measuring bar [41] is schematically shown in Fig.3.



10

11 **Fig. 3.** Schematic representation of the setup for measuring forces resisting penetration in
12 the inverse experiment.

13

14 A container filled with soil (sand) is accelerated up to the required velocities and
15 impacted against a stationary striker fixed on a measuring bar. The impact velocity and the
16 material properties are to be such that no plastic strains should occur in the bar. An elastic strain
17 pulse $\varepsilon(t)$ is formed in the bar. Registering this pulse on the surface of the bar makes it possible
18 to determine the force F , acting on the striker upon its interaction with the medium, according to
19 the known relation $F(t) = E\varepsilon(t)S_0$, where E is the elastic modulus of the bar and S_0 is its cross-
20 section area.

21 Thus, in this method, the task of measuring the forces is considerably simplified and
22 reduced to registering an elastic strain pulse in the bar, using strain gauges. The setup

1 implementing this method is schematically depicted in Fig. 3. In the present version of the
2 inverse experiment, a soil container is accelerated using a 57 mm caliber gas-gun with a two-
3 diaphragm breech mechanism, which makes it possible to provide stable and readily controlled
4 impact velocities in the range from 50 to 500 m/s, using air compressed up to 15 MPa, and up to
5 ~1000 m/s, when using compressed helium.

6 The container is a thin-walled cartridge, filled with soil. To prevent the soil from spilling
7 in the process of preparation of the experiment and during acceleration of the container, the front
8 end of the container is sealed with 0.01 mm-thick PET film. The film is fixed and secured against
9 the surface of the soil with a vinyl-resin ring.

10 The impact velocity of the container was determined using two electric-contact
11 transducers located in the orifices of the barrel, made in the vicinity of the muzzle. A 1.5 m-long
12 20 mm-diameter steel rod with yield strength larger than 2000 MPa was used as a measuring bar.
13 The steel measuring bar had density $\rho = 8050 \text{ kg/m}^3$, Young's modulus $E = 186 \text{ GPa}$. One of the
14 ends of the measuring bar has a threaded orifice housing a cylindrical striker with a head of
15 appropriate geometry. The bar is located at a certain distance from the barrel muzzle, so that the
16 impact occurs immediately after the container entirely leaves the barrel. The stand on which the
17 bar is located has adjusting supports, which are used to provide axisymmetric interaction. The
18 rear end of the bar rests against a special damper, preventing it from displacing and damping the
19 impact energy. Impact takes place inside a vacuum chamber, to which the gun barrel is
20 connected, and into which the measuring bar with its head is introduced. The cylindrical part of
21 the heads was 19.8 mm in diameter, with the radius of the hemisphere equal to 10 mm, and were
22 made of steel with a yield strength larger than 1800 MPa.

23 24 **2.3. The conditions of the experiments**

25 For the inverse tests, cylindrical containers made of aluminum alloy were used, which
26 had the following dimensions: outer diameter 56.8 mm, inside diameter 54 mm, bottom

1 thickness 2 mm, filling depth 65 mm. To prevent sand from strewing out during the test, the sand
2 surface in the container was fixed with a 0.01 mm thickness PET film.

3 Both experiments were conducted with dry and water saturated (wet) sandy mixture of a
4 natural composition, from which particles larger than 1 mm and smaller than 0.1 mm had been
5 removed. The particle size distribution of dry sand mixture is presented in Table 1.

6
7 **Table 1.** Particle size distribution of the sand used in experiments.

| Mean particle diameter (mm) | The granules lie in the range between the size value shown in the given column and the size value in the column immediately to the left of that. | | | | | |
|-----------------------------|--|------|-------|------|------|-----|
| | 0.63 | 0.4 | 0.315 | 0.2 | 0.16 | 0.1 |
| % finer by mass | 5.0 | 21.5 | 13.2 | 38,8 | 11.6 | 9.9 |

8

9 The dry sand filled into the container was compacted layer-by-layer until reaching an
10 average density of about 1750 ± 50 kg/m³. In the tests of water-saturated sand, the containers
11 filled with dry sand were poured with a certain amount of water until the sand was completely
12 saturated. Further saturation resulted in the formation of a water layer over the surface of the
13 sand, so the excess water was poured off. The containers were weighed again to determine the
14 density of the water-saturated sand and its moisture content relative to its initial density. The
15 average density of the water-saturated (wet) natural mixture was 2080 ± 50 kg/m³.

16

17 **3. Analyzing the problem of a spherical cavity expanding in a soft soil**

18

19 **3.1. Analytical solution in the assumption of incompressibility of the medium behind the** 20 **shock wave front**

21 *3.1.1. Formulating an initial boundary-value problem for a system of partial differential*
22 *equations.*

1 A mathematical model of a soil medium is described by a system of differential equations
 2 expressing the laws of continuity and balance of linear momentum, which in spherical Eulerian
 3 coordinates can be written as:

$$4 \quad \rho \left(\frac{\partial v}{\partial r} + 2 \frac{v}{r} \right) = - \left(\frac{\partial \rho}{\partial t} + v \frac{\partial \rho}{\partial r} \right), \quad \frac{\partial \sigma_r}{\partial r} + 2 \frac{(\sigma_r - \sigma_\theta)}{r} = - \rho \left(\frac{\partial v}{\partial t} + v \frac{\partial v}{\partial r} \right), \quad (1)$$

5 where ρ is density in a deformed state, v is velocity, σ_r and σ_θ are radial and circumferential
 6 components of Cauchy stress tensor (which are assumed positive in compression), r is the radial
 7 coordinate.

8 The system of partial differential equations (1) is closed by finite relations determined
 9 from the experiment:

$$10 \quad \sigma_r = f_1(\theta), \quad \sigma_r - \sigma_\theta = f_2(\theta) \quad (2)$$

11 where ρ_0 is initial density of the medium, $\theta = 1 - \rho_0/\rho$ is volumetric strain.

12 Functions f_1 and f_2 define the equation of state and the plasticity condition of the soil
 13 medium.

14 Along the boundary of a cavity whose radius is $R_0 = Vt$, expanding from point
 15 ($R_0|_{t=0} = 0$), the velocity V is assigned, the outer surface of spherical layer R_∞ is free from
 16 stresses, and at the initial time both velocity and stresses in the medium are equal to zero:

$$17 \quad v(R_0, t) = V, \quad \sigma_r(R_\infty, t) = 0, \quad v(r, 0) = \sigma_r(r, 0) = 0. \quad (3)$$

18 The solution of the problem is constructed in the plastic yield region bounded by radii
 19 $r = Vt$ and $r = ct$ and adjacent to the region of unperturbed medium (the elastic damping of
 20 the soft soil medium is neglected).

21 *3.1.2. Formulating a boundary-value problem for a system of first-order partial*
 22 *differential equations.*

23 Following [1 – 9], self-similar variable $\xi = r/ct$ is used in the solution of the problem.

24 The partial derivatives in time and space are defined as follows:

$$\frac{\partial v}{\partial r} = \frac{dv}{d\xi} \frac{\partial \xi}{\partial r} = \frac{1}{ct} \frac{dv}{d\xi}, \quad \frac{\partial v}{\partial t} = \frac{dv}{d\xi} \frac{\partial \xi}{\partial t} = -\frac{\xi}{t} \frac{dv}{d\xi}, \quad \frac{\partial \sigma_r}{\partial r} = \frac{1}{ct} \frac{d\sigma_r}{d\xi}, \quad \frac{\partial \sigma_r}{\partial t} = -\frac{\xi}{t} \frac{d\sigma_r}{d\xi}.$$

The system of partial differential equations (1) is transformed into a system of ordinary differential equations (ODE):

$$\rho \left(\frac{1}{ct} \frac{dv}{d\xi} + 2 \frac{v}{\xi ct} \right) = - \left(-\frac{\xi}{t} + \frac{v}{ct} \right) \rho^2 \frac{d\theta}{\rho_0 d\xi}, \quad (4)$$

$$\frac{1}{ct} \frac{d\sigma_r}{d\xi} + 2 \frac{f_2(\theta)}{\xi ct} = -\rho \left(-\frac{\xi}{t} + \frac{v}{ct} \right) \frac{dv}{d\xi},$$

where $\sigma_r = f_1(\theta)$, as it follows from equation of state (2).

System (4) is transformed, assuming a time $t > 0$:

$$\frac{1}{c} \frac{dv}{d\xi} + 2 \frac{v}{\xi c} = \frac{(\xi - v/c) d\theta}{(1-\theta) d\xi}, \quad \frac{1}{\rho c^2} \frac{d\sigma_r}{d\xi} + 2 \frac{f_2(\theta)}{\xi \rho c^2} = (\xi - v/c) \frac{1}{c} \frac{dv}{d\xi} \quad (4)$$

For $\xi=1$, Rankine-Hugoniot's jump conditions are used on the shock wave:

$$[\rho]c - [\rho v] = 0, \quad [\rho v]c - [\rho v^2 + \sigma_r] = 0 \quad (5)$$

In (5), square brackets designate difference of the values to the left and to the right of the discontinuity, and c is the propagation velocity of the discontinuity. The values to the left and to the right of the discontinuity will be designated as ρ_s, v, σ and ρ_0, v_0, σ_0 , respectively.

In view of its smallness the elastic precursor in a soft soil medium can be neglected. Then,

assuming $v_0 = \sigma_0 = 0$, one has $(\rho_s - \rho_0)c = \rho_s v$, $\rho_s v c = \rho_s v^2 + \sigma$,

or $1 - \rho_0/\rho_s \equiv \theta_s = v/c$, $v/c - (v/c)^2 = \sigma/\rho_s c^2$.

It is also assumed that, at high cavity expansion velocities, the density of the soft soil is low; then system (4) is considered in the assumption of incompressibility of the medium, i.e., when equalities $d\theta/d\xi = 0$ or $\theta = const$ do hold.

1 In equations (4), the value of the volumetric strain is taken to be $\theta \equiv \theta_s$ and $\rho \equiv \rho_s$. The
 2 fact that density retains its value ρ_s on the shock wave amounts to the assumption of
 3 incompressibility of the medium behind the shock wave front. Values of ρ_s and θ_s are
 4 determined for every value of cavity expansion velocity.

5 Having chosen $U = v/c$ and $S = \sigma/\rho_s c^2$ as dimensionless variables, one gets the
 6 following system of ODE (the prime designates differentiation with respect to ξ)

$$7 \quad U' + 2 \frac{U}{\xi} = 0, \quad S' + 2 \frac{\tilde{f}_2}{\xi} = (\xi - U)U', \quad \varepsilon < \xi < 1 \quad (6)$$

8 and boundary conditions

$$9 \quad U(\xi = \varepsilon) = \varepsilon, \quad (7)$$

$$10 \quad U(\xi = 1) = \theta_s, \quad S(\xi = 1) = U - U^2 = \theta_s - \theta_s^2,$$

11 where the following definitions are introduced: $\varepsilon = V/c$ is a dimensionless coordinate,
 12 corresponding to the cavity boundary, $\tilde{f}_2(\cdot) = f_2(\cdot)/\rho_s c^2$ is a dimensionless function in the
 13 plasticity condition.

14 *3.1.3. Solution of the boundary-value problem for a system of ODE with Mohr-Coulomb*
 15 *yield criterion.*

16 To solve the boundary-value problem for a system of two first-order ordinary differential
 17 equations, (6), (7), it is necessary to provide functions f_1 and f_2 of the equation of state of the
 18 medium.

19 Experiments [45, 46] indicate that dynamic compressibility of soil media is characterized
 20 by a shock adiabat in the form of a linear relation:

$$21 \quad U_s = C_0 + su_p, \quad (8)$$

1 correlating plane shock wave velocity U_s and velocity of particles behind the wave front, u_p .

2 Here, C_0 corresponds to sonic velocity in the medium at zero pressure.

3 Relations (8) were obtained experimentally in shock-wave experiments for the conditions
4 of uniaxial strain. In the present formulation of the spherical cavity expansion problem, the
5 shockwave velocity and the plastic wave velocity are taken to be equal to $U_s \equiv c$. This is
6 another simplifying assumption, mentioned earlier in [1].

7 Substituting relation (8) into Rankine-Hugoniot's equations (5), one obtains $v = \theta c$,
8 $\sigma_r = \rho_0 v c = \rho_0 \theta c^2$; relation (8) will become $c = C_0 + s \theta c$, $c = C_0 / (1 - s \theta)$. The final
9 form of the relation between stress σ_r and volumetric strain θ will be
10 $f_1(\theta) \equiv \rho_0 C_0^2 \theta (1 - s \theta)^{-2}$ [45], which has been used earlier in computations [49, 50]. In this
11 formulation, parameter s characterizes compression strength of the soil. The barotropic
12 approximation applied to soil media is justified by the fact that, at pressures up to 10 GPa, the
13 relative thermal volumetric expansion is an order of magnitude smaller than the total relative
14 change of the volume.

15 Taking account of conditions (8) on the shock wave, boundary conditions (7) can be
16 rewritten as follows:

17
$$U(\xi = \varepsilon) = \varepsilon, U(\xi = 1) = (1 - C_0/c)/s, \quad (9)$$

18 The first equation of system (1.6) is an equation with branching variables
19 $dU/U = -2d\xi/\xi$, the solution of which yields $U = c_1/\xi^2$. Constant c_1 is determined from
20 the first boundary condition in (9) as $c_1 = \varepsilon^3$, and the dimensionless velocity has the following
21 form:

22
$$U = \varepsilon^3/\xi^2 \quad (10)$$

1 To determine the unknown value ε , taking into account the second boundary condition in
 2 relations (9) $\varepsilon^3 = (1 - C_0/c)/s = (1 - C_0V/Vc)/s = (1 - \varepsilon/M)/s$, the following cubic equation
 3 is obtained:

$$4 \quad \varepsilon^3 + \frac{\varepsilon}{sM} - \frac{1}{s} = 0, \quad (11)$$

5 where $M = V/C_0$. The coefficients in equation (11) depend only on the parameters of the shock
 6 adiabat of the medium C_0 , s and cavity expansion velocity V .

7 An exact solution of equation (11) according to Cardano's formula has the following
 8 form:

$$9 \quad \varepsilon = \sqrt[3]{1/(2s) + q} + \sqrt[3]{1/(2s) - q}, \quad (12a)$$

10 where the definition $q = \sqrt{(2s)^{-2} + (3sM)^{-3}}$ has been introduced.

11 A linear approximation to ε , which follows from equation (11), when using Taylor's

12 expansion $\varepsilon = \frac{1}{\sqrt[3]{s}} \left(1 + \left(-\frac{\varepsilon}{M} \right) \right)^{1/3} \approx \frac{1}{\sqrt[3]{s}} \left(1 - \frac{\varepsilon}{3M} \right)$, yields

$$13 \quad \varepsilon \approx 3M / (1 + 3M\sqrt[3]{s}) \quad (12b)$$

14 Using the definition $\varepsilon = V/c$, one obtains

$$15 \quad c = V \left(\sqrt[3]{1/(2s) + q} + \sqrt[3]{1/(2s) - q} \right)^{-1}, \quad (13a)$$

$$16 \quad c \approx \sqrt[3]{s}V + C_0/3 \quad (13b)$$

17 Earlier, a solution of the form of (13a) was obtained in the cylindrical cavity expansion
 18 problem [1].

19 It is further assumed that the plasticity criterion of the medium is described by Mohr-
 20 Coulomb's law $f_2(\cdot) \equiv \tau_0 + \kappa p = \tau_0 + \mu \sigma_r$, where τ_0 is cohesion, κ is internal friction
 21 coefficient, $p = (\sigma_r + 2\sigma_\theta)/3$ is pressure, $\mu = \kappa/(1 + 2\kappa/3)$.

1 The second equation of system (6) and the boundary condition when taking into account
 2 solution (10) and the yield criterion will be written as:

$$3 \quad S'+2\frac{T_0+\mu S}{\xi} = -2\left(\xi - \frac{\varepsilon^3}{\xi^2}\right)\frac{\varepsilon^3}{\xi^3} = -2\frac{\varepsilon^3}{\xi^2} + 2\frac{\varepsilon^6}{\xi^5}, \quad S(\xi=1) = \varepsilon^3 - \varepsilon^6 \quad (14)$$

4 where $T_0 = \tau_0 / \rho_s c^2$.

5 Transferring the terms containing S in equation (14) into the left-hand side and the rest of
 6 the terms into the right-hand side, and multiplying the left-hand and the right-hand sides of the
 7 equation by $\xi^{2\mu}$:

$$8 \quad \left(S'+2\frac{\mu S}{\xi}\right)\xi^{2\mu} = \left(-2\frac{T_0}{\xi} - 2\frac{\varepsilon^3}{\xi^2} + 2\frac{\varepsilon^6}{\xi^5}\right)\xi^{2\mu},$$

9 one obtains, after some transformations, an equation with branching variables,
 10 $d(S\xi^{2\mu}) = \left(-2T\xi^{2\mu-1} - 2\varepsilon^3\xi^{2\mu-2} + 2\varepsilon^6\xi^{2\mu-5}\right)d\xi$, the solution of which depends on
 11 the arbitrary variable c_2

$$12 \quad S = -\frac{T_0}{\mu} - 2\frac{\varepsilon^3}{(2\mu-1)\xi} + \frac{\varepsilon^6}{(\mu-2)\xi^4} + c_2\xi^{-2\mu}$$

13 Taking into account boundary conditions (14), the dimensionless stress takes the form:

$$14 \quad S(\xi) = -\frac{T_0}{\mu} - 2\frac{\varepsilon^3}{(2\mu-1)\xi} + \frac{\varepsilon^6}{(\mu-2)\xi^4} + \left(\frac{T_0}{\mu} + 2\frac{\varepsilon^3}{(2\mu-1)} - \frac{\varepsilon^6}{(\mu-2)} + \varepsilon^3 - \varepsilon^6\right)\xi^{-2\mu} \quad (15a)$$

15 Equation (15a) is not defined for $\mu=0$ and $\mu=0.5$. In these cases, a solution can be
 16 obtained by passing to the limit in (15a) for μ tending to 0 and 0.5, respectively

$$17 \quad S(\xi) = -2T_0 \ln \xi - \varepsilon^3 \left(1 - \frac{2}{\xi}\right) - \frac{\varepsilon^6}{2} \left(1 + \frac{1}{\xi^4}\right), \quad \mu = 0 \quad (15b)$$

$$18 \quad S(\xi) = -2T_0 \left(1 - \frac{1}{\varepsilon}\right) - \varepsilon^3 \left(2\frac{\ln \xi}{\xi} - \frac{1}{\xi}\right) - \frac{\varepsilon^6}{3} \left(\frac{1}{\xi} + \frac{2}{\xi^4}\right), \quad \mu = 0.5 \quad (15c)$$

1 In a dimensional form, the stress as a function of the self-similar variable has the
 2 following form:

$$\begin{aligned}
 \sigma_r(\xi) = & \tau_0 \left(\frac{\xi^{-2\mu} - 1}{\mu} \right) + \\
 & + \frac{\rho_0 V^2 \varepsilon}{1 - \varepsilon^3} \left(\frac{2}{(2\mu - 1)} \left(\frac{\xi^{-2\mu+1} - 1}{\xi} \right) + \frac{\varepsilon^3}{(\mu - 2)} \left(\frac{1 - \xi^{-2\mu+4}}{\xi^4} \right) + (1 - \varepsilon^3) \xi^{-2\mu} \right)
 \end{aligned} \quad (16)$$

4 Equations (16) were derived using the equality $\rho_s = \rho_0 / (1 - \varepsilon^3)$.

5 The dimensionless stress on the cavity wall ($\xi = \varepsilon$), depending on the values of internal
 6 friction coefficient μ , is defined as:

$$S = T_0 \left(\frac{\varepsilon^{-2\mu} - 1}{\mu} \right) + \frac{3\varepsilon^2}{(2\mu - 1)(\mu - 2)} + \varepsilon^3 \left(\frac{2}{(2\mu - 1)} - \frac{\varepsilon^3}{(\mu - 2)} + 1 - \varepsilon^3 \right) \varepsilon^{-2\mu},$$

8 In a dimensional form, the stress σ_C on the boundary of the cavity expanding at a
 9 velocity V , has the following form:

$$\sigma_C \equiv \sigma_r(\xi = \varepsilon) = \tau_0 \left(\frac{\varepsilon^{-2\mu} - 1}{\mu} \right) + \quad (17a)$$

$$+ \frac{\rho_0 V^2}{1 - \varepsilon^3} \left(\frac{3}{(\mu - 2)(2\mu - 1)} + \frac{2\mu + 1}{2\mu - 1} \cdot \varepsilon^{1-2\mu} - \frac{\mu - 1}{\mu - 2} \cdot \varepsilon^{4-2\mu} \right),$$

$$\sigma_r(\xi = \varepsilon) = -2\tau_0 \ln \varepsilon + \frac{\rho_0 V^2}{1 - \varepsilon^3} \left(3/2 - \varepsilon - \varepsilon^4/2 \right), \quad \mu = 0 \quad (17b)$$

$$\sigma_r(\xi = \varepsilon) = 2\tau_0 (\varepsilon^{-1} - 1) + \frac{\rho_0 V^2}{1 - \varepsilon^3} \left(1/3 - 2 \ln \varepsilon - \varepsilon^3/3 \right), \quad \mu = 0.5 \quad (17c)$$

13 In equations (16), (17), the value of ε is determined based on equations (12). The
 14 relations for stresses obtained by substituting equations (12a) and (12b) are in what follows called
 15 *rigid-plastic* and *linearized*, respectively. Thus, final relations have been obtained, which make it
 16 possible to determine the stress in a medium with Mohr-Coulomb's plasticity condition.

17 *3.1.4. Solution of a boundary-value problem for a system of ODE with Mohr-Coulomb*
 18 *Tresca-limit yield criterion.*

1 The plasticity function for Mohr-Coulomb's condition, with the account of the limitation
 2 for Tresca's maximal value of the yield strength has the following form:

$$3 \quad f_2 \equiv \begin{cases} \tau_0 + \mu\sigma_r, & 0 < \sigma_r \leq \sigma_M, \\ \tau_M, & \sigma_r > \sigma_M \end{cases}$$

4 where $\sigma_M = (\tau_M - \tau_0)/\mu$. In a dimensionless form, this equation is:

$$5 \quad \tilde{f}_2 \equiv \begin{cases} T_0 + \mu S, & 0 < S \leq S_M, \\ T_M, & S > S_M \end{cases}$$

6 where dimensionless values $T_M = \tau_M / \rho_s c^2$, $S_M = (T_M - T_0)/\mu$ are introduced.

7 Stress S monotonically decreases with the dimensionless coordinate ξ changing from ε
 8 to 1, i.e., the minimal stress value is achieved at $\xi=1$. The value of cavity expansion
 9 velocity V_M , at which $S(\xi=1) = S_M$, is then determined.

10 From the relations on the shock wave for $\xi=1$ it follows that $\sigma_r = \rho_0 c v = \rho_0 c^2 \theta$.

11 The values of shock wave velocity, volumetric strain and ε , corresponding to $V = V_M$, will be
 12 designated as c_M , θ_M and ε_M , respectively. To determine c_M , formula (13b) will be used,
 13 yielding

$$14 \quad c_M = \sqrt[3]{sV_M + C_0/3}, \quad \theta_M = \varepsilon_M^3 = \frac{V_M^3}{c_M^3}, \quad \sigma_M = \rho_0 c_M^2 \theta_M = \rho_0 \frac{V_M^3}{c_M}.$$

15 Then, to determine V_M , the following cubic equation is obtained:

$$16 \quad \left(\frac{\tau_M - \tau_0}{\mu} \right) \left(\sqrt[3]{sV_M + C_0/3} \right) = \rho_0 V_M^3 \quad (18a)$$

17 In a similar way, the maximal stress value is achieved at $\xi=\varepsilon$. Symbol V_0 will
 18 designate the value of cavity expansion velocity, at which equalities $S(\xi=\varepsilon) = S_M$ or
 19 $\sigma_r(\xi=\varepsilon) = \sigma_M$ hold. Substituting value $V = V_0$ into equation (17), $\sigma_M = \sigma_r(\xi=\varepsilon)|_{V=V_0}$,

20 the following nonlinear equation for determining V_0 is obtained:

$$\begin{aligned}
1 \quad & \frac{\tau_M - \tau_0}{\mu} = \frac{\tau_0}{\mu} \left(1 - \varepsilon_0^{-2\mu}\right) + \\
& + \frac{\rho_0 V_0^2}{1 - \varepsilon_0^3} \left(\frac{3}{(\mu - 2)(2\mu - 1)} + \frac{2\mu + 1}{2\mu - 1} \cdot \varepsilon_0^{1-2\mu} - \frac{\mu - 1}{\mu - 2} \cdot \varepsilon_0^{4-2\mu} \right), \quad (18b)
\end{aligned}$$

2 where definitions $\varepsilon_0 = V_0/c_0$, $c_0 = \sqrt[3]{sV_0} + C_0/3$ have been introduced.

3 For a cavity expansion velocity varying in the interval $V_0 < V < V_M$, it is necessary to
4 find the value of the dimensionless coordinate $\xi = \xi_M$, at which the value of the dimensionless
5 stress is $S(\xi = \xi_M) = S_M$.

6 Finally, the dimensionless stress will be defined as:

$$7 \quad S(\xi) = \begin{cases} -\frac{T_0}{\mu} - 2\frac{\varepsilon^3}{(2\mu-1)\xi} + \frac{\varepsilon^6}{(\mu-2)\xi^4} + & \left(0 < \varepsilon < \varepsilon_0\right) \cup \\ & \left(\varepsilon \leq \xi \leq 1\right) \\ + \left(\frac{T_0}{\mu} + 2\frac{\varepsilon^3}{(2\mu-1)} - \frac{\varepsilon^6}{(\mu-2)} + \varepsilon^3 - \varepsilon^6\right) \xi^{-2\mu}, & \left(\varepsilon_0 < \varepsilon < \varepsilon_M\right); \\ & \left(\xi_M \leq \xi \leq 1\right); \\ S_M + T_M \ln\left(\frac{\xi_M}{\xi}\right)^2 + 2\varepsilon^3\left(\frac{1}{\xi} - \frac{1}{\xi_M}\right) - \frac{\varepsilon^6}{2}\left(\frac{1}{\xi^4} - \frac{1}{\xi_M^4}\right), & \varepsilon_0 \leq \varepsilon \leq \varepsilon_M, \\ & \varepsilon \leq \xi \leq \xi_M; \\ -2T_M \ln \xi - \varepsilon^3\left(1 - \frac{2}{\xi}\right) - \frac{\varepsilon^6}{2}\left(1 + \frac{1}{\xi^4}\right), & \varepsilon > \varepsilon_M, \\ & \varepsilon \leq \xi \leq 1. \end{cases} \quad (19)$$

8 Dimensional stress along the cavity boundary $\sigma_C \equiv S(\xi = \varepsilon)\rho_s c^2$

$$9 \quad \sigma_r(V) = \begin{cases} \frac{\tau_0}{\mu} \left(\varepsilon^{-2\mu} - 1\right) + & 0 < V < V_0; \\ + \frac{\rho_0 V^2}{1 - \varepsilon^3} \left(\frac{3}{(\mu - 2)(2\mu - 1)} + \frac{2\mu + 1}{2\mu - 1} \cdot \varepsilon^{1-2\mu} - \frac{\mu - 1}{\mu - 2} \cdot \varepsilon^{4-2\mu} \right), & \\ \sigma_M + \tau_M \ln\left(\frac{\xi_M}{\varepsilon}\right)^2 + \frac{\rho_0 V^2}{1 - \varepsilon^3} \left(\frac{3}{2} - \frac{2\varepsilon}{\xi_M} + \frac{\varepsilon^4}{2\xi_M^4} \right), & V_0 \leq V \leq V_M, \quad (20) \\ -2\tau_M \ln \varepsilon + \frac{\rho_0 V^2}{1 - \varepsilon^3} \left(\frac{3}{2} - \varepsilon - \frac{\varepsilon^4}{2} \right), & V > V_M. \end{cases}$$

1 In equations (19), (20) the value of ε is determined in the same way, using equations (12).
 2 Thus, the final relations are obtained, which make it possible to determine the stress in a medium
 3 with Mohr-Coulomb Tresca-limit yield criterion.

4

5 **3.2. Numerical solution of the problem in a complete formulation**

6 *3.2.1. Formulating an initial boundary-value problem for a system of partial differential*
 7 *equations.*

8 A mathematical model of a soil medium is described by differential equation system (1),
 9 which is closed by an invariant relation between pressure and volumetric strain:

$$10 \quad p = f_3(\theta) \equiv K\theta + O(\varepsilon^2), \quad (21)$$

11 where K is the elastic bulk modulus (i.e. the modulus of volumetric compression).

12 It is assumed that in the region bounded by radii $R_0 = Vt$ and $r = ct$, the medium is
 13 plastically deformed. In the adjacent region of elastic deformation, which is bounded by
 14 coordinate $r = c_e t$, the stress tensor components are related to strains by Hooke's law with
 15 elastic moduli K and G , where $c_e = \sqrt{(K + 4G/3)/\rho_0}$ is the plane shock wave propagation
 16 velocity, and G is the shear modulus.

17 A solution of a one-dimensional problem of spherical cavity expansion in the region of
 18 plastic deformation will be now constructed. In view of the spherical symmetry and of the fact
 19 that the first invariant of the deviator tensor is equal to zero, $s_r + 2s_\theta = 0$, and if yield
 20 condition $\sigma_r - \sigma_\theta = f_2(\theta)$ holds, one obtains $s_r = 2f_2(\theta)/3$, where s_r and s_θ are radial
 21 and circumferential components of the stress deviator tensor.

22 System of partial differential equations (1) for σ_r and v will be written as follows:

$$23 \quad \frac{1}{K_1} \left(\frac{\partial \sigma_r}{\partial t} + v \frac{\partial \sigma_r}{\partial r} \right) + (1 - \theta) \left(\frac{\partial v}{\partial r} + \frac{2v}{r} \right) = 0, \quad \frac{\partial \sigma_r}{\partial r} + \frac{2f_2(\sigma_r)}{r} = -\frac{\rho_0}{1 - \theta} \left(\frac{\partial v}{\partial t} + v \frac{\partial v}{\partial r} \right), \quad (22)$$

24 where $1 - \theta = 1 - f_1^{-1}(\sigma_r)$, $\sigma_r = f_1(\theta) \equiv f_3(\theta) + \frac{2}{3}f_2(\theta)$, $K_1 = \frac{\partial f_1(\theta)}{\partial \theta}$

1 On the boundary of the expanding cavity of radius $R_0 = V_0 t$, velocity V is assigned, outer
 2 surface of the spherical layer R_∞ is free from stresses, the velocity and stresses in the medium at
 3 the initial time are equal to zero:

$$4 \quad v(R_0, t) = V, \quad \sigma_r(R_\infty, t) = 0, \quad v(r, 0) = \sigma_r(r, 0) = 0. \quad (23)$$

5 *3.2.2. Formulation of a boundary-value problem for a system of first-order ordinary differential*
 6 *equations.*

7 A self-similar solution of the system for variable $\xi = \frac{r}{ct}$ will be considered, and

8 dimensionless variables $U = \frac{v}{c}$, $S = \frac{\sigma_r}{\rho_0 c^2}$ will be introduced together with the following

9 notations: $\tilde{f}_1(\theta) = \frac{f_1(\theta)}{\rho_0 c^2}$, $\tilde{f}_2(\theta) = \frac{f_2(\theta)}{\rho_0 c^2}$, $\tilde{K}_1 = \frac{\partial \tilde{f}_1(\theta)}{\partial \theta}$. The partial derivatives in time and

10 space are defined similarly to Section 3.1.2.

11 As a result of the substitution, the system of partial differential equations (22) is
 12 transformed into a system of ordinary differential equations:

$$13 \quad U' + 2 \frac{U}{\xi} = \frac{(\xi - U)}{(1 - \theta)\tilde{K}_1} S', \quad S' + 2 \frac{\tilde{f}_2}{\xi} = \frac{(\xi - U)}{1 - \theta} U', \quad (24)$$

14 where $1 - \theta = 1 - \tilde{f}_1^{-1}(S)$, and prime denotes differentiation with respect to ξ .

15 Boundary conditions (23) for equation system (24) are defined depending on the relation
 16 of velocities c and c_e , and value $\alpha = c/c_e$. For $0 < \alpha < 1$, the boundary conditions are
 17 defined by an elastic solution (Appendix A). For $\alpha \geq 1$, Hugoniot's jump conditions (5) are
 18 used, from which it follows that $\theta = v/c$, $v/c = \sigma/\rho_0 c^2$ or, in dimensionless variables,
 19 $U = S = \theta$.

20 Finally, the boundary value problem for a system of two first-order ordinary differential
 21 equations, written in a normal form, is as follows:

$$U' = \frac{2(U\tilde{K}_1 + \tilde{f}_2\varphi)}{\xi(\varphi^2 - \tilde{K}_1)}, \quad S' = \frac{2\tilde{K}_1(\tilde{f}_2 + U\varphi)}{\xi(\varphi^2 - \tilde{K}_1)}, \quad \varepsilon < \xi < 1, \quad (25)$$

$$U(\xi = \varepsilon) = \varepsilon,$$

$$U(\xi = 1) = \begin{cases} U^e, & \alpha < 1 \\ \theta_1, & \alpha \geq 1 \end{cases}, \quad S(\xi = 1) = \begin{cases} S^e, & \alpha < 1 \\ \theta_1, & \alpha \geq 1 \end{cases},$$

where $\varphi = (\xi - U)/(1 - \theta)$, and θ_1 is the solution of equation $\tilde{f}_1(\theta) = \theta$.

Equation system (25) includes the unknown parameter c , propagation velocity of the interface between the elastic and plastic regions or of the plastic shock wave front. The unknown velocity c is determined iteratively, as long as boundary condition $|U(\xi = \varepsilon) - \varepsilon| < \delta$ is satisfied to an assigned accuracy δ . At each iteration step, the fourth-order-accurate Runge-Kutta numerical method is used for self-similar variable ξ changing from elastic-plastic interface ($\xi=1$) to cavity boundary ($\xi=\varepsilon$).

4. Analyzing the accuracy of the approximate solution

4.1. Parametric analysis of the cavity problem solution with Mohr-Coulomb yield criterion

The problem of spherical cavity expanding at a constant velocity from a zero radius in an infinite nonlinearly compressible medium is considered. Compressibility of the medium is characterized by linear relation (8) between shock wave velocity and mass velocity of the particles of the medium. Resistance of the medium to shear is assigned by Mohr-Coulomb's linear relation. Cavity expansion velocity, internal friction coefficient μ , and parameter of dynamic compression strength s are varied.

4.1.1. Formation of a plastic shock wave.

As it was noticed in Section 3.2, the solution of the problem in the plastic region is continuous at the transition to the elastic region, for $c > c_e$ a plastic shock wave is formed, which propagates through the unperturbed space. Further, two choices of the parameters of the

1 equation of state (EOS) of a medium with known stress-volumetric strain (shock adiabat)
 2 relations and Mohr-Coulomb's yield criterion are considered as an illustration, which are listed
 3 in the Table 2. In what follows, media with EOS1 and EOS2 will be considered.

4

5 **Table 2.** Parameters of the EOS of media 1 and 2.

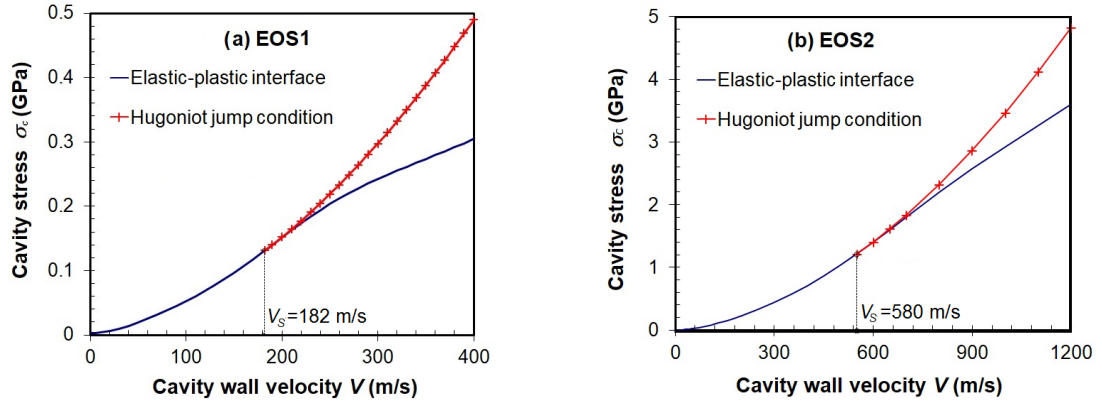
| No | ρ_0 , kg/m ³ | K , MPa | G , MPa | c_e , m/s | C_0 , m/s | s | σ_0 , MPa | k | μ |
|----|---------------------------------|--------------|--------------|----------------|----------------|-----|---------------------|-----|-------|
| 1 | 1730 | 220 | 115 | 465 | 460 | 2.3 | 0.042 | 1.0 | 0.6 |
| 2 | 2080 | 4570 | 1147 | 1713 | 1700 | 3.4 | 0.021 | 0.5 | 0.375 |

6

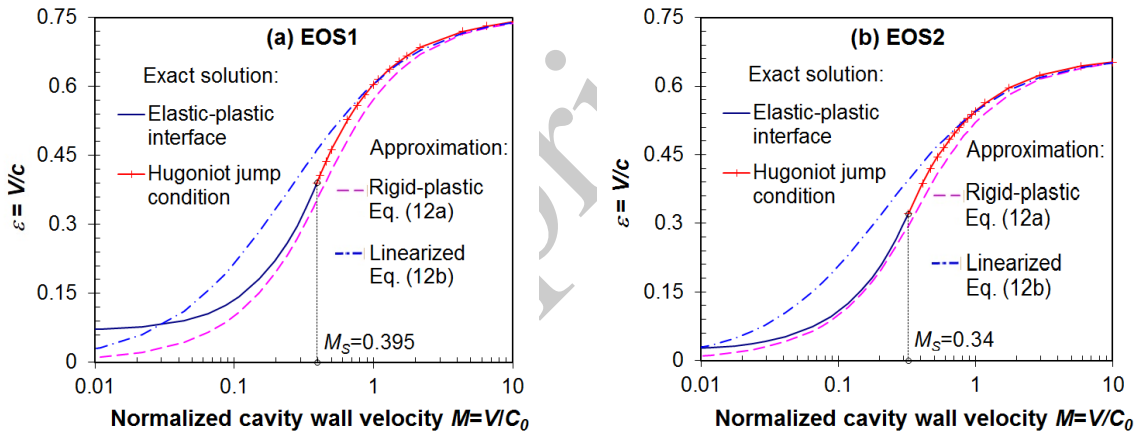
7 The curves in Fig. 4 correspond to the results of the solution of the boundary-value
 8 problem for a system of ODE (Section 3.2, Eqs. (25)), using the fourth-order-accurate Runge-
 9 Kutta method. In what follows, this solution will be called 'exact solution'.

10 It is found that a shock wave is formed at cavity expansion velocities $V = V_s$ (marked in
 11 dotted lines), $V_s = 182$ m/s and 550 m/s for media with EOS1 and EOS2, respectively. In the
 12 vicinity of these values, the solution curves have second-order tangency.

13 In Fig. 5, velocity is represented on a logarithmic scale, the dashed line corresponds to
 14 the value of the dimensionless cavity expansion velocity $M_s \equiv V_s / C_0$, at which a single plastic
 15 shock wave is formed ($M_s = 0.395$ and $M_s = 0.340$ for the media with EOS1 and EOS2,
 16 respectively).



1 **Fig. 4.** Stress at the boundary of a cavity expanding at velocity V for the media with
 2 EOS1 (a) and EOS2 (b): elastic-plastic solution for $V \leq V_s$ (solid line) and the solution
 3 indicating the formation of a single plastic shock wave propagating through the unperturbed
 4 medium (the crossed solid line) for $V > V_s$.



5 **Fig. 5.** Dimensionless parameter ε as a function of cavity expansion velocity in
 6 relation to elastic wave velocity for the media with EOS1 (a) and EOS2 (b): exact
 7 generalized solution including elastic-plastic interface (the solid blue line) at $M \leq M_s$ and
 8 formation of a plastic shock wave (the solid red line with a cross) at $M > M_s$, approximated
 9 *rigid-plastic* solution (12a) (the dotted line) and *linearized* solution (12b) (the dot-dash line).
 10

11 The exact solution in Fig. 5 demonstrates the limitation of parameter ε when the cavity
 12 expansion velocity tends to infinity ($\varepsilon < 0.758$ and $\varepsilon < 0.663$ for EOS1 and EOS2 respectively)
 13 and to zero ($\varepsilon > 0.066$ and $\varepsilon > 0.023$ again for media with EOS1 and EOS2, respectively). The
 14 approximate solutions according to formulas (12) are limited from above ($\varepsilon < 1/\sqrt[3]{s}$). The

1 dimensional stress value on the cavity wall also remains limited at velocities close to zero: for
 2 media with EOS1, the stress does not exceed 2.3 MPa, and for a medium with EOS2 it does not
 3 exceed 1.13 MPa. The value of ε , obtained using formula (13a), is close enough to the exact
 4 solution, except for the region with $M < 0.1$, the solution according to linearized formula (13b)
 5 tends to the exact solution only at $M > 0.4$.

6 The evaluation of the minimal stress on the cavity wall, required for its propagation
 7 (critical pressure P_c [10]) is now considered. Earlier, an equation for a critical pressure in a
 8 compressed linearly elastic medium with Tresca's plasticity condition was obtained:

$$9 \quad P_c = \frac{2}{3} \tau_0 \left(1 + \ln \frac{E}{3(1-\nu)\tau_0} \right) \quad (26)$$

10 where E is Young's modulus, and ν is Poisson's coefficient.

11 To determine the critical pressure in a medium with Mohr-Coulomb's plasticity criterion,
 12 the second equation of system (24) is transformed into an equation for the dimensional pressure.
 13 Taking into account that elastic-plastic interface velocity $c = O(V)$, at $V \rightarrow 0$ yields Cauchy's
 14 problem:

$$15 \quad \frac{d\sigma_r}{d\xi} + 2 \frac{\tau_0 + \mu\sigma_r}{\xi} = 0, \quad \varepsilon \leq \xi \leq 1, \quad \sigma_r(\xi = 1) = 2\tau_0/3, \quad (27)$$

16 where the boundary conditions are defined based on the second equation in (A9) for $\alpha \ll 1$.

17 The solution of Cauchy's problem (27) is a function $\sigma_r(\xi)$ which, for $\xi = \varepsilon$, defines
 18 the critical pressure

$$19 \quad P_c = \frac{2}{3} \tau_0 \varepsilon^{-2\mu} + \tau_0 \left(\frac{\varepsilon^{-2\mu} - 1}{\mu} \right). \quad (28a),$$

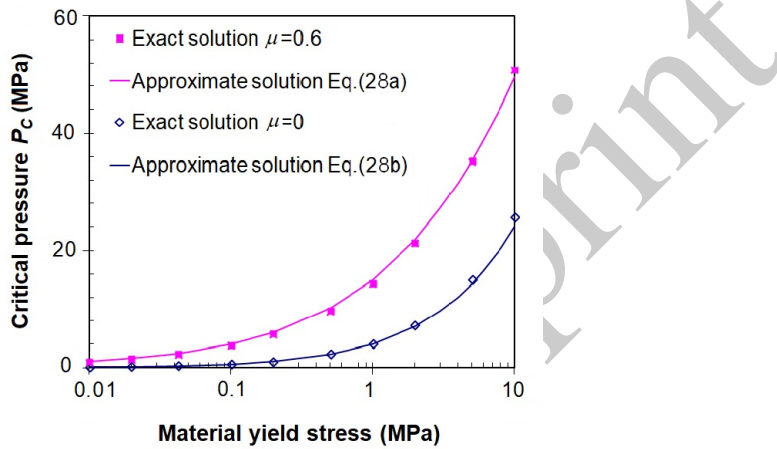
20 The value of such critical pressure for $\mu = 0$ can be obtained by passing to the limit
 21 $\mu \rightarrow 0$ in (28a):

$$22 \quad P_c = \frac{2}{3} \tau_0 \left(1 + \ln \varepsilon^{-3} \right) \quad (28b)$$

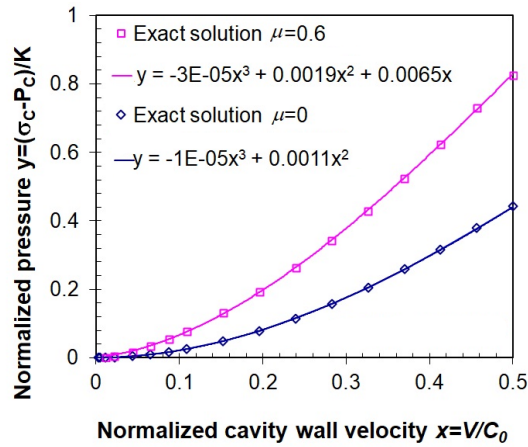
1 Considering that value ε weakly depends on the change in internal pressure, equation (26) will
 2 be used for determining ε , assuming $\varepsilon = \sqrt[3]{3(1-\nu)\tau_0/E}$. Thus, equation (28a) will be a
 3 generalization of the known equation (26) for the case of Mohr-Coulomb's yield criterion.

4 Fig. 6 presents the values of critical pressure on the cavity wall, obtained numerically for
 5 various levels of the initial value of yield strength in a medium where a logarithmic scale is used
 6 for the yield stress. Good applicability of equation (28a) is noticed for τ_0 changing by three
 7 orders of magnitude, as well as the growth of critical pressure with an increasing internal
 8 pressure.

9



10 **Fig.6.** Critical pressure P_c for a medium with EOS1 as a function of the initial value
 11 of the yield strength τ_0 : exact numerical solution (the solid lines) and solution according to
 12 formulas (28) (the markers).
 13



1

2

3

4

5

6

7

8

9

10

11

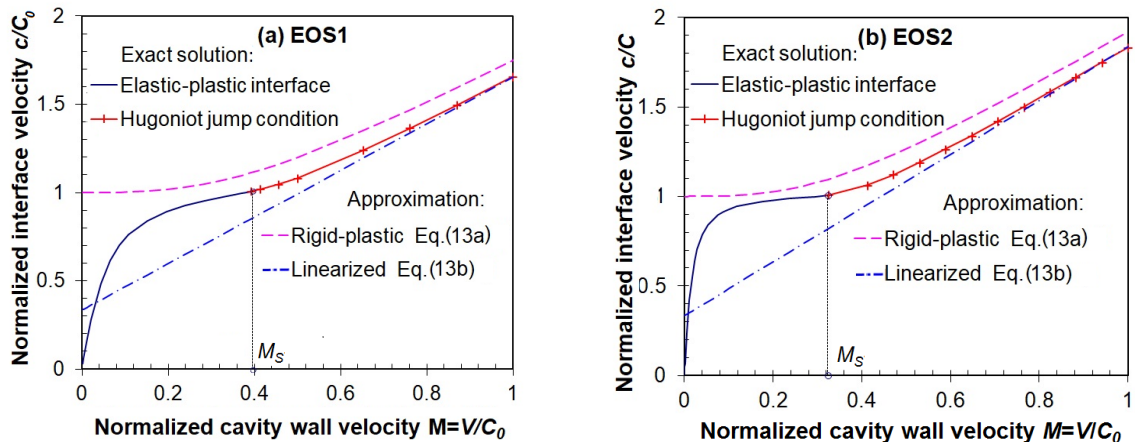
12

13

Fig.7. Normalized pressure on the cavity wall as a function of cavity expansion velocity in a medium with EOS1: exact numerical solution (the markers) and an approximation using the least squares method (the solid lines).

The polynomial approximations in Fig. 7 are functions of the form $(\sigma_C - P_C)/K_0 = -A_3(V/C_0)^3 + A_2(V/C_0)^2$ for the case $\mu = 0$ and $(\sigma_C - P_C)/K_0 = -B_3(V/C_0)^3 + B_2(V/C_0)^2 + B_1(V/C_0)$ for the case $\mu = 0.6$. It can be noticed that a linear member appearing in the approximating polynomial is determined by accounting for the internal pressure in the framework of Mohr-Coulomb's yield criterion.

The *linearized* solution (13b) in Fig. 8 appears to be closer to the exact solution for $M > 0.4$, than the *rigid-plastic* solution according to Cardano's formula (13a).

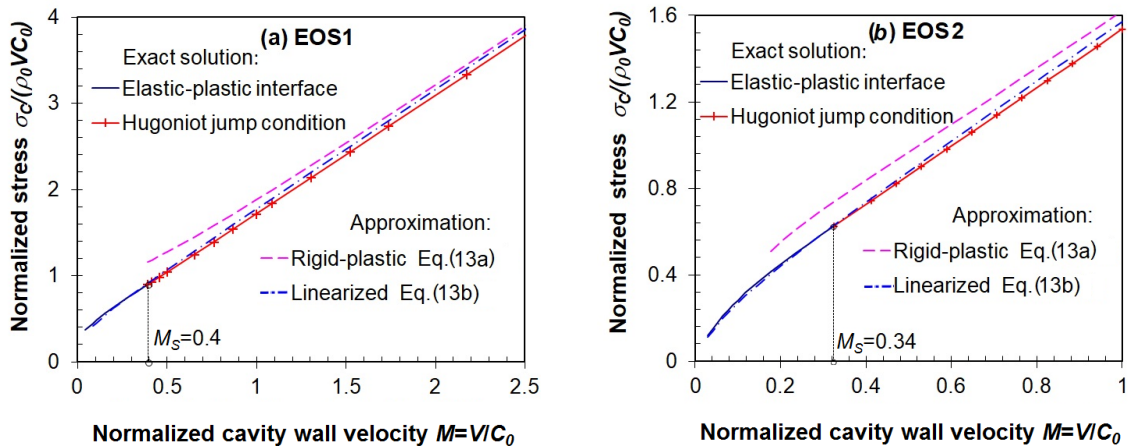


1 **Fig. 8.** Normalized propagation velocities of the elastic-plastic interface as a function
 2 of cavity expansion velocity for the media with EOS1 (a) and EOS2 (b): (the definition of the
 3 curves is the same as in Fig. 5).

4
 5 It has to be noticed that solving the problem without accounting for the formation of a
 6 plastic shock wave results in the limitation of the elastic-plastic interface at high cavity
 7 expansion velocities (the solid line in Fig.8), which agrees with the results earlier obtained in
 8 [16]. The continuation of the solution, concentrating on the single plastic shock wave (the solid
 9 line with a cross in Fig. 8) is closer to the physical picture of wave propagation.

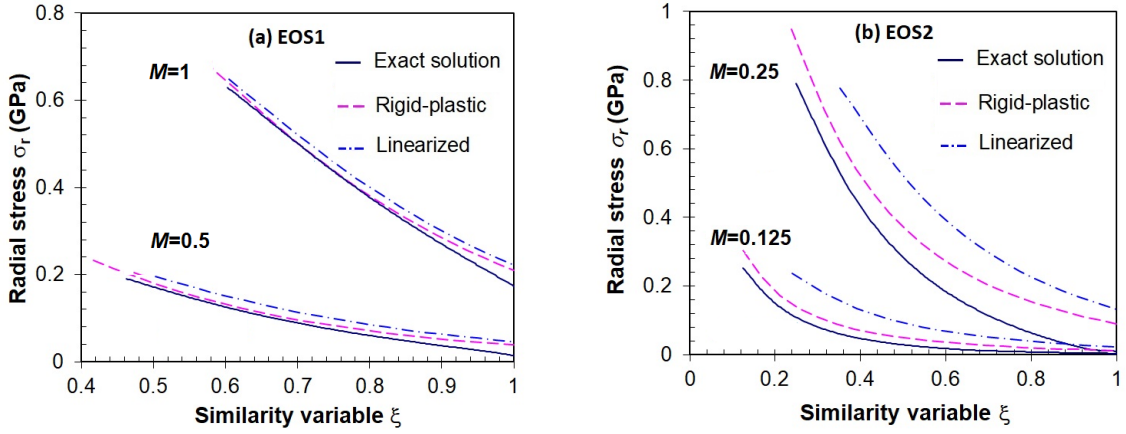
10 The approximate solutions in Fig. 9 were obtained using formulas (12a), (17a) and (12b),
 11 (17a), respectively. The approximate linearized solution agrees well with the exact solution in a
 12 complete formulation over a fairly wide range of cavity expansion velocities up to $M=0.1$. Like
 13 the exact solution, the dimensionless linearized solution has a nonlinear character at $M<0.4$, and
 14 at $M>0.4$ can be represented by a linear relation.

15 The good agreement between the approximate linearized and the exact solutions can be
 16 explained if stress distributions in the medium as a function of the dimensionless coordinate is
 17 considered.



18 **Fig. 9.** Dimensionless relations between stress on the cavity wall expanding at velocity
 19 V for the media with EOS1 (a) and EOS2 (b): (the definition of the curves is the same as in Fig.
 20 5).

21



1 **Fig. 10.** Stress distribution in the medium as a function of similarity variable ξ at the
 2 dimensionless cavity expansion for velocities $M=0.5$ and $M=1.0$ for a medium with EOS1
 3 (a), $M=0.125$ and $M=0.250$ for the medium with EOS2 (b): the solid, dotted and dot-dash
 4 lines correspond to the exact generalized solution, the *rigid-plastic* and *linearized* rigid-
 5 plastic solutions, respectively.

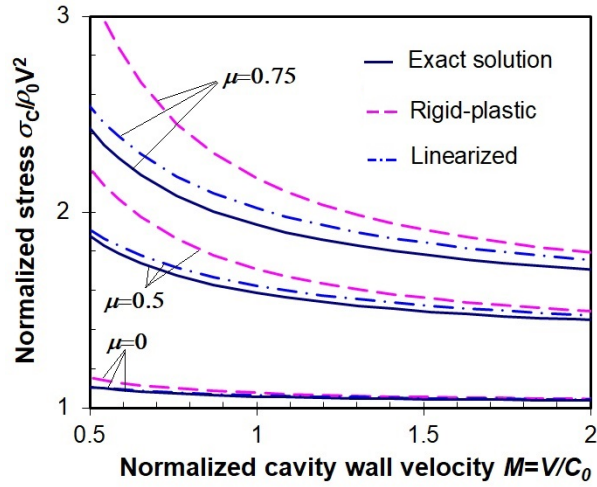
6
 7 It is evident in Fig. 10 that the computations of stress using equation (12a) for
 8 determining \mathcal{E} and equation (13a) for determining shock wave velocity generally give closer
 9 results than those obtained using the linearized formula (13b). However, maximal stress values
 10 in the vicinity of the cavity, obtained using formulas (12b), (17b) (the dot-dash line in Fig. 10),
 11 tend to be closer to the exact value. The formal continuation of solution (13) into the region with
 12 $M < 0.4$ for a medium with EOS2 leads to an error of 13% and 16% in defining the stress at the
 13 cavity boundary. Errors in determining stresses using formulas (12b), (17b) substantially
 14 decrease with an increasing cavity expansion velocity.

15 4.1.2. Evaluation of stress at the cavity wall.

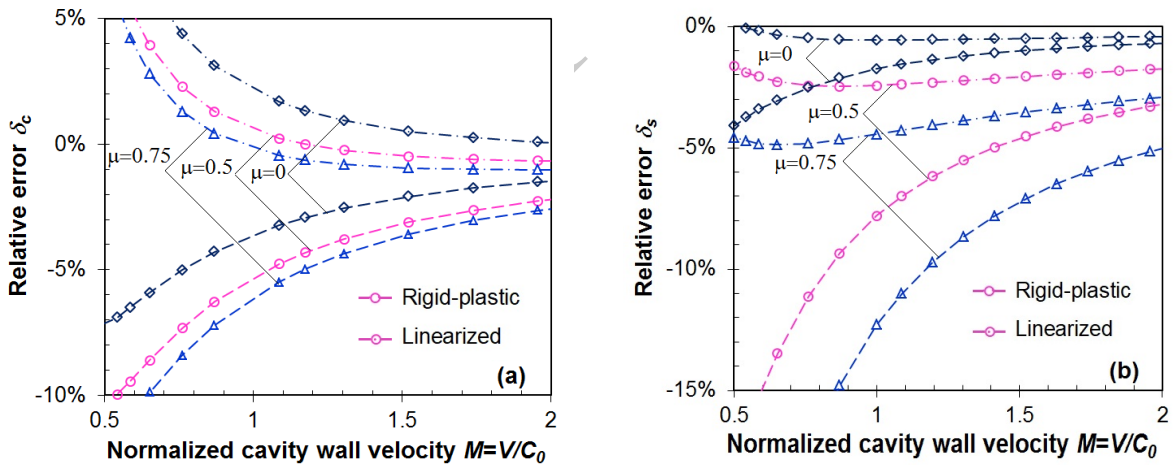
16 In what follows, the normalized stresses obtained in the framework of the problem of
 17 spherical cavity expansion, by varying the internal friction coefficient, are compared; the
 18 remaining parameters correspond to the material with EOS1.

19 It follows from Fig. 11 that the difference between the stresses obtained exactly and
 20 approximately decreases with the cavity expansion velocity. This corroborates the earlier
 21 conclusion that linear relation (13b) of shock wave velocity as a function of cavity expansion

1 velocity is more accurate in determining normal stress at the cavity wall than the exact solution
 2 using Cardano's formulas (13a).



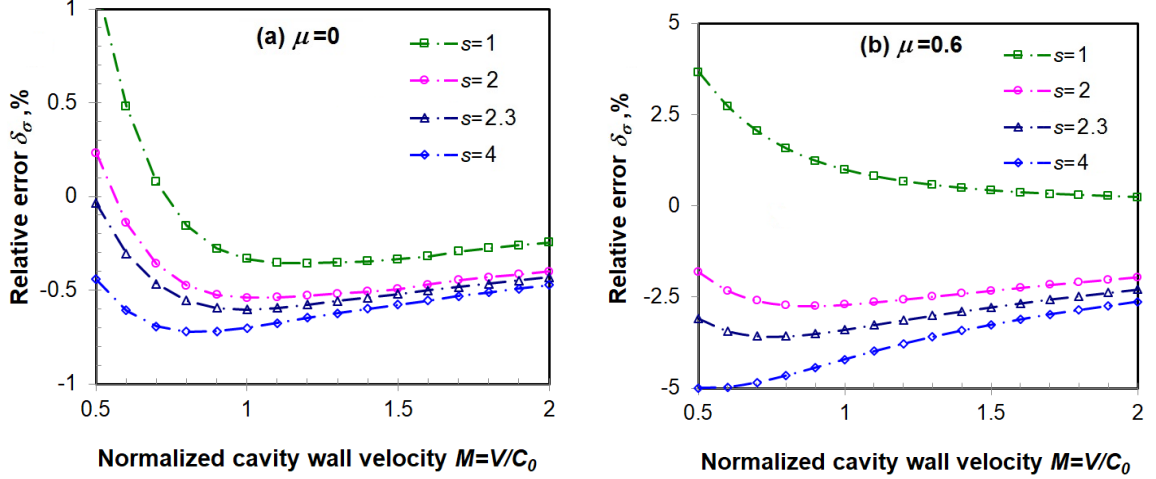
3
 4 **Fig. 11** Normalized stresses at the cavity wall as a function of dimensionless
 5 expansion velocity, obtained for the internal friction coefficient values $\mu=0$; $\mu=0.5$; $\mu=0.75$.
 6 (definitions are the same as in Figs. 9, 10).



8 **Fig. 12.** Relative error in determining the shock wave front velocity (a) and the stress
 9 at the cavity wall (b) for $\mu=0$, $\mu=0.5$ and $\mu=0.75$.

10 This is connected with a summation of errors of opposite sign. The difference between the
 11 approximate and exact solutions increases with μ , the character of the curves remaining the same.
 12 The minimal error of the approximate solutions is observed for a value of the internal friction
 13 coefficient close to 0.
 14

1



2 **Fig. 13.** Relative errors in determining the cavity wall stress for various values of
 3 compression strength coefficient s of the soil for internal friction coefficient $\mu = 0$ (a) and μ
 4 $= 0.6$ (b) as a function of relative cavity expansion velocity $M = V / C_0$.

5

6 Fig. 12(a) depicts relative errors in determining the plastic shock wave velocity for various
 7 values of internal friction coefficient $\delta_c = (c - c_{a,b}) / c \cdot 100\%$, where c is the exact solution, and
 8 c_a and c_b are determined from formulas (13a) and (13b). The relative errors for the stress at the
 9 cavity wall depicted in Figs. 12(b), are determined in a similar way. The relative errors for
 10 approximate linearized formulas (17b), (12b) are significantly lower than those using Cardano's
 11 formulas (12a). The errors are also observed to decrease with an increasing cavity expansion
 12 velocity. Thus, velocities and stresses at the wall of a spherical cavity, expanding at a constant
 13 velocity from zero radius in a soil medium with a known shock adiabat, are determined using
 14 formulas (13b) and (17), (12b) with an error less than 5% at relative cavity expansion velocities
 15 $M = V / C_0 > 0.4$ and when the variation of the internal friction coefficient is in the range [0;
 16 0.75].

17 The error in Fig. 13 was determined in a standard way: $\delta_\sigma = (\sigma_C - \sigma_b) / \sigma_C \cdot 100\%$,
 18 where σ_C is the exact solution, and σ_b is determined using formulas (17), (12b). It can be seen
 19 that the errors in determining the stress at the wall of the spherical cavity, expanding at a

1 constant velocity in a soft medium, using linearized formula (12b) and formula (17b) do not
 2 exceed 5% at relative cavity expansion velocities $M = V/C_0 > 0.5$ and compression strength
 3 parameter S changing in a fairly wide range [1; 4] for admissible values of the internal friction
 4 coefficient.

5 Determining the plastic shock wave velocity using formula (13b) and the stress at the
 6 cavity wall using equations (12b), (17b) can formally be extended onto the range $M < 0.5$.

7 It is evident from Fig. 14 that at relative cavity expansion velocity $M < 0.5$ the error in
 8 determining the shock wave velocity increases up to 50%. For stresses calculated at the cavity
 9 wall, the errors do not exceed 5% over the entire velocity range, and only for large values of the
 10 internal friction coefficient ($\mu=0.75$) and small relative cavity expansion velocities, the errors
 11 increase up to 10%. The obtained estimations show that equation (17) and the linearized
 12 equations (12b), (13b) can be further used for approximating stresses at the cavity wall when
 13 analyzing problems of penetration into soil media.

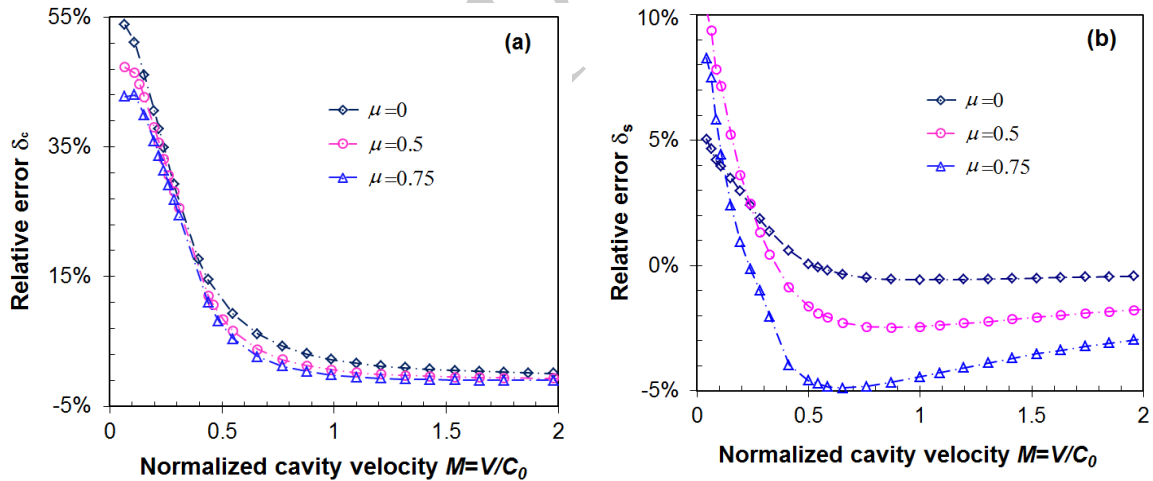


Fig. 14 Error in determining shock wave front velocity (a) and cavity wall stress (b) using the linearized rigid-plastic solution for the values of $\mu=0$, $\mu=0.5$ and $\mu=0.75$.

14

15 **5. Determining the force resisting penetration of a rigid sphere into sand**

16

17 **5.1. Parameters of the equation of state of the soil medium**

1 As it is known, the equation of state of a soft soil includes a shock adiabat, a plasticity
 2 condition, as well as elasticity moduli K and G of the initial part of the deformation curve.
 3 Representing the shock adiabat in the form of linear relation (8) makes it possible to correlate
 4 stress σ_r and volumetric strain θ in conditions of uniaxial deformation:

$$5 \quad f_1(\theta) \equiv \rho_0 C_0^2 \theta (1 - s\theta)^{-2} \quad (29)$$

6 Resistance of the medium to shear is defined by a bilinear relation between yield stress
 7 and pressure:

$$8 \quad f_2(p) \equiv \sigma_0 + kp / (1 + kp / \Delta\sigma), \quad \Delta\sigma = \sigma_1 - \sigma_0 \quad (30)$$

9 Coefficients σ_0 , σ_1 and k in (30) characterize cohesion, maximal value of yield stress and
 10 tangent of the internal friction angle of the soil.

11 For the “pressure-volumetric strain” relation, $f_3(\theta)$, the following function of the form
 12 (29) is used:

$$13 \quad p = f_3(\theta) \equiv \rho_0 a^2 \theta (1 - b\theta)^{-2}, \quad (31)$$

14 where the unknown parameters a and b are found by using the least squares method.

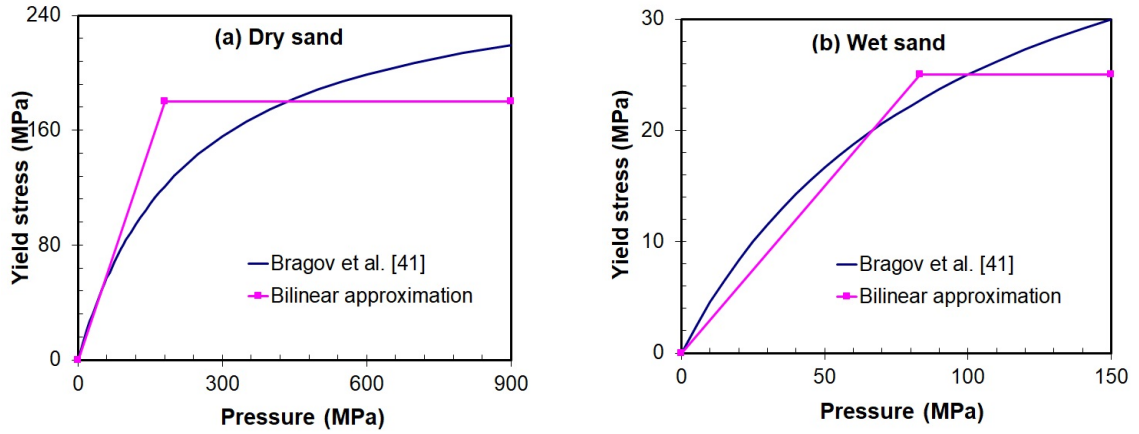
15 The shock adiabats parameters C_0 and s for dry and wet sand were obtained in our
 16 plane-wave shock experiments. These parameters were close to those obtained earlier in the
 17 inverse impact experiment technique by using a measure bar with flat end [41]. The following
 18 Table 3 lists the parameter values of the equation of state of dry and water-saturated sands

19

20 **Table 3.** Parameters of EOS for sand of different water saturation.

| N_0 | w , % | ρ_0 , kg/m ³ | C_0 , m/s | s | a , m/s | b | σ_0 , MPa | k | σ_1 , MPa |
|-------|------------|---------------------------------|----------------|-----|--------------|-----|---------------------|-----|------------------|
| 1 | 0 | 1730 | 460 | 2.3 | 340 | 2.6 | 0.1 | 1.2 | 275 |
| 2 | 20 | 2080 | 1700 | 3.4 | 1620 | 3.6 | 0.1 | 0.5 | 50 |

1



2 **Fig. 15.** Bilinear relations between yield stress and pressure for dry (a) and wet soils
 3 (b) and Mohr-Coulomb-Tresca's bilinear approximation.

4

5 Fig. 15 presents curves of nonlinear yield criterion (30) as approximated by the bilinear
 6 relations of Mohr-Coulomb's with Tresca's-limit yield criterion

$$7 \quad f_2 \equiv \begin{cases} \tau_0 + kp = \tau_0 + \mu\sigma_r, & 0 < \sigma_r \leq \sigma_M, \\ \tau_M, & \sigma_r > \sigma_M \end{cases} \quad (32)$$

8

9 **Table 4.** Parameters of yield criterion (32) for dry and wet sand.

| No | $\tau_0,$ | k | μ | $\tau_M,$ | $\sigma_M,$ |
|----|-----------|-----|-------|-----------|-------------|
| | MPa | | | MPa | MPa |
| 1 | 0.042 | 1.0 | 0.6 | 180 | 300 |
| 2 | 0.021 | 0.3 | 0.25 | 25 | 1000 |

10

11 The parameters of the elastic portion of the deformation diagram and the shock adiabat of
 12 dry and wet sands are those previously presented in Table 2.

13

14 **5.2. Analytical solution of the cavity problem with Mohr-Coulomb Tresca's limit yield**
 15 **criterion**

1 In Fig. 16, the cavity expansion velocities are 400 and 250 m/s for dry (a) and wet (b)
 2 sands, respectively. The values of parameters V_0 and V_M , determined using formulas (18), and
 3 the values of other parameters are summarized in the Table 5:

4

5 **Table 5.** Limits of the chosen ranges in equations (19) and (20).

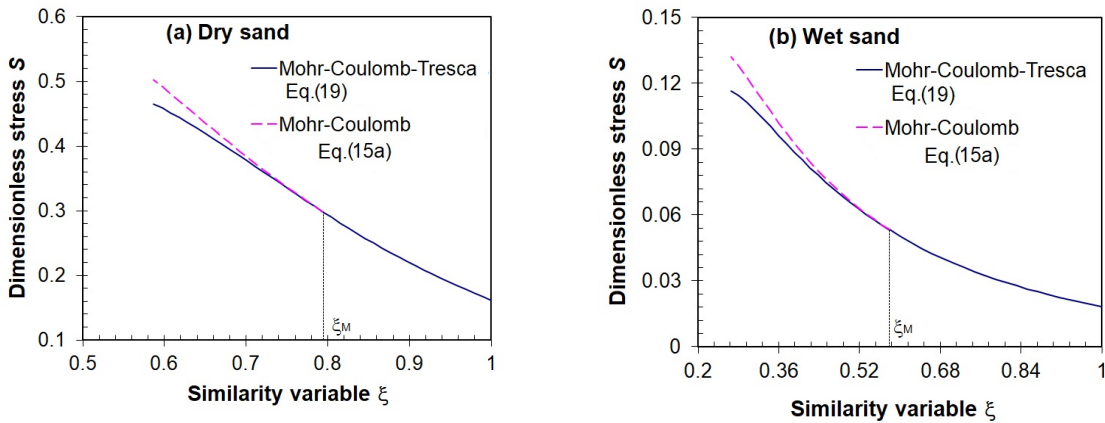
| No | V_0 , m/s | V_M , m/s | ε_0 | ε_M | V , m/s | ξ_M | S_M |
|----|----------------|----------------|-----------------|-----------------|--------------|---------|-------|
| 1 | 296 | 528 | 0.544 | 0.607 | 400 | 0.795 | 0.298 |
| 2 | 150 | 380 | 0.19 | 0.305 | 250 | 0.58 | 0.053 |

6

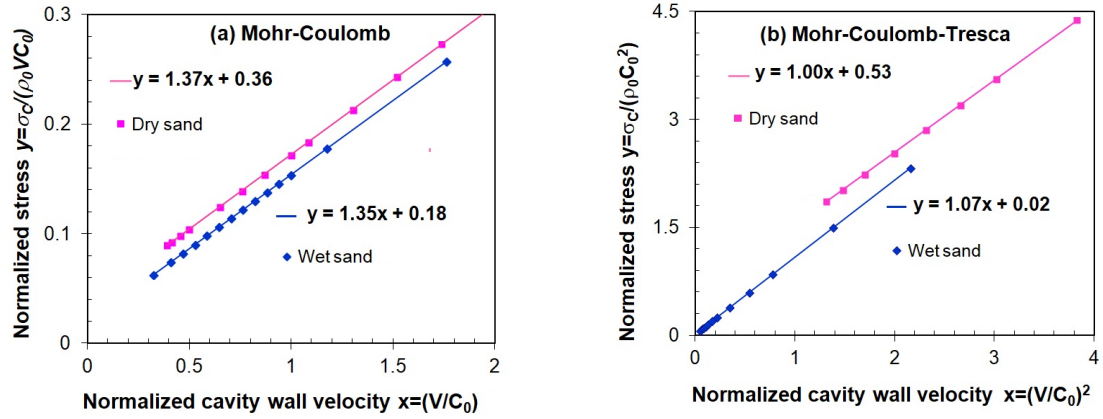
7 In Table 5, the first and second lines correspond to dry and wet sand, respectively.

8 In Fig. 17, the markers represent normalized cavity wall stresses as a function of
 9 normalized expansion velocities under high pressures. Using Mohr-Coulomb's yield criterion
 10 (a), the stresses were found according to formula (17a) for $M > 0.4$; the parameters of the
 11 equation of state are listed in Table 2. With Mohr-Coulomb-Tresca's yield criterion (b), formula
 12 (17b) was used with $\tau_0 = \tau_M$, $V > V_M$; the parameters of the equation of state are listed in
 13 Table 3.

14

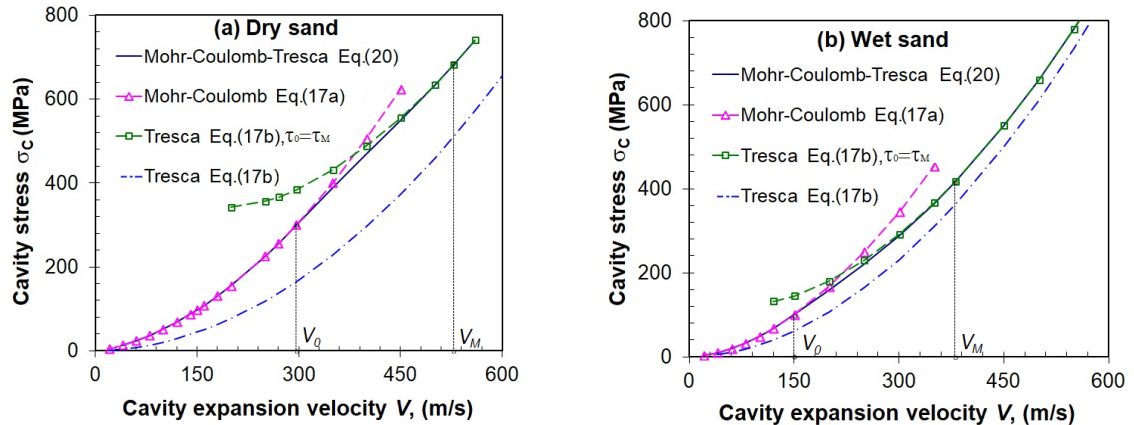


1 **Fig. 16.** Distribution of dimensionless stresses as a function of self-similar coordinate
 2 in dry (a) and wet (b) sand for Mohr-Coulomb-Tresca's yield criterion (the solid line) and
 3 Mohr-Coulomb's criterion (the dotted line).
 4



5 **Fig. 17.** Normalized cavity wall stresses as a function of normalized cavity expansion
 6 velocities when using Mohr-Coulomb's (a) and Mohr-Coulomb Tresca's limit (b) yield
 7 criterions in dry and wet sand (squares and diamonds, respectively) and linear
 8 approximations using the least squares method (solid lines).
 9

10 It can be seen that when using Mohr-Coulomb's yield criterion, the relation between
 11 stresses acting on the cavity wall and the velocity is $\sigma_r / \rho_0 = a_2 V^2 + b_1 V$ (see also [51]),
 12 whereas when Tresca's yield criterion is used for $\tau_0 = \tau_M$, $V > V_M$, the relation is
 13 $\sigma_r / \rho_0 = a_2 V^2 + a_0$; besides, $a_0 \approx 0$ for the wet soil.



1 **Fig. 18.** Approximation of the cavity wall stress as a function of cavity expansion
 2 velocity in dry (a) and wet (b) sands: the solid line, the dotted line with triangles, the dash-
 3 dot lines and the dashed line with squares correspond to the results obtained using equations
 4 (20), (17a), (17b) and (17b) for $\tau_0 = \tau_M$.

5

6 It can be seen in Fig. 18 that the cavity wall stresses in the medium with Mohr-Coulomb-
 7 Tresca's yield criterion can, accurately enough for engineering purposes, be determined without
 8 using equations (19), (20), by employing interpolation over the cavity expansion velocity range
 9 $V_0 \leq V \leq V_M$.

10

11 **5.3. Comparing the numerical and experimental results**

12 The force acting on a spherical head projectile penetrating into soil at constant velocity
 13 U_0 , equal to impact velocity, is determined by integrating stresses over the contact surface and
 14 is related with the form and penetration velocity of the projectile as

$$15 \quad F = -2S \int_{-1}^z \left(\sigma_n z + \sigma_\tau \sqrt{1 - z^2} \right) dz \quad (33a)$$

16 where $S = \pi R^2$ is the cross-section area of the sphere, $z = -1 + U_0 t / R$ is the current penetration
 17 depth, related with projectile radius R , axis z is directed along the symmetry axis of the
 18 projectile and against its motion, $-1 \leq z \leq 0$, t is current penetration time.

19 Angle φ is now introduced, which is counted from the apex of the sphere in the direction
 20 of the free surface corresponding to dimensionless penetration depth $z = \cos \varphi$. Equation (33a)
 21 can be transformed as follows:

$$22 \quad F = 2S \int_0^\varphi (\sigma_n \cos \varphi + \sigma_\tau \sin \varphi) \sin \varphi d\varphi . \quad (33b)$$

1 According to the Cavity Expansion Model (CEM), normal stress acting on the surface of
 2 the projectile is identified with pressure acting on the wall of the expanding spherical cavity. As
 3 it was shown above, this pressure can be represented in the form of a quadratic relation

$$4 \quad \sigma_n / \rho_0 = a_2 u^2 + b_1 u, \quad (34)$$

5 where $u = -U_0 z$ is the normal component of the penetration velocity vector, a_2 , b_1 are
 6 constant coefficients depending on the physical-mechanical properties of the medium, the
 7 geometry of the striker and other components.

8 Tangent stresses on the surface of the body moving through the medium will be defined
 9 according to Coulomb's friction model

$$10 \quad \sigma_\tau = k_f \sigma_n, \quad (35)$$

11 where k_f is a constant coefficient of surface friction.

12 After integrating equation (33), taking into account (34), (35), resistance to a spherical
 13 penetrator as a function of impact velocity will have the following form:

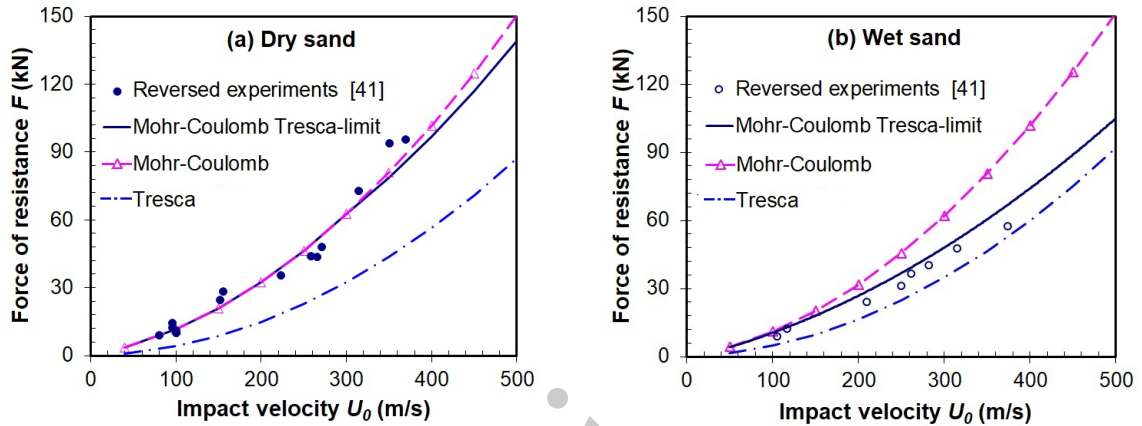
$$14 \quad F = AU_0^2 + BU_0, \quad A = a_2(A_1 + k_f A_2)\rho_0 S, \quad B = b_1(B_1 + k_f B_2)\rho_0 S,$$

$$15 \quad A_1 = \frac{(1 - \cos^4 \varphi)}{2}, \quad A_2 = \frac{(\varphi - 2 \sin \varphi \cos^3 \varphi + \sin \varphi \cos \varphi)}{4}, \quad B_1 = \frac{2(1 - \cos^3 \varphi)}{3}, \quad B_2 = \frac{2 \sin^3 \varphi}{3} \quad (36)$$

16 Substituting into (36) the values of φ , equal to a flow separation angle, φ^* , yields the
 17 maximum values of the force resisting penetration in the framework of CEM, taking into account
 18 surface friction.

19 The flow separation angle was taken to be $\varphi^* = \pi/3$, the friction coefficient for dry
 20 sand was $k_f = 0.4$, and for wet sand $k_f = 0.2$. These values were assumed to be proportional to
 21 the internal friction coefficient, i.e., remained constant at $u < V_0$. At $u > V_M$, the values of the
 22 sliding friction coefficient were assumed to be equal to $k_f = 0$, over the interval $V_0 < u < V_M$ a
 23 linear interpolation was used.

1 Fig. 19 demonstrates good agreement between the approximation results and the
 2 experimental data for both dry and water-saturated sand without introducing any correcting
 3 coefficients. In the velocity range, for which the experimental data for dry sand were obtained
 4 (impact velocities up to 400 m/s), Mohr-Coulomb's yield criterion is true, whereas Tresca's limit
 5 comes to produce significant effects at impact velocities over 500 m/s.



6 **Fig. 19.** Resistance force to penetration of a rigid spherical striker into dry (a) and wet
 7 (b) sand as a function of impact velocity: the inverted experiment [41] (the dark and light
 8 dots) and the approximation using the solution of the cavity expansion problem (the
 9 definition of the curves is the same as in Fig. 18).

10
 11 The use of Mohr-Coulomb's with Tresca's-limit yield criterion is more justified for wet
 12 sand. At low impact velocities (up to 200 m/s), internal friction plays an important role, whereas
 13 at higher velocities the limitation of the yield strength in the framework of Tresca's yield
 14 criterion manifests itself.

15 Indeed, high-speed penetrators are here considered, where resistance to shear of the soil
 16 medium can be neglected. Normal pressure on the surface moving at velocity U_0 will be
 17 expressed by equation (17b) without the first addend: $\sigma_r = \rho_0 U_0^2 \left(\frac{3}{2} - \varepsilon - \varepsilon^4/2 \right) / (1 - \varepsilon^3)$. The
 18 stress on the contact surface will be written as $\sigma_r = \frac{1}{2} C_D \rho_0 U_0^2$, where C_D is resistance
 19 coefficient. Then, assuming that $\varepsilon = 1/\sqrt[3]{s}$ (upper bound), the evaluation of coefficient C_D as a

1 function of shock adiabat parameter s will be: $C_D = (3 - (2 + 1/s)/\sqrt[3]{s})/(1 - 1/s)$. With s varying
2 in the range $1 < s < 4$, the resistance coefficient changes in the range $2 < C_D < 2.11$, which is
3 close enough to the results of [52], where the values of the coefficient of resistance to a flat-
4 nosed penetrator, $C_D \approx 2$, were obtained.

5

6 **6. Conclusions**

7 1. The linear shock adiabats $U_s - u_p$ for both dry and wet sand were obtained in our
8 plane-wave shock experiments. These data were close to those obtained earlier in the inverse
9 impact experiment technique by using a measure bar with a flat end.

10 2. As applied to the problem of the penetration of rigid bodies into soft soils, a self-
11 similar analytical solution has been obtained for a one-dimensional problem of the expansion of
12 a spherical cavity from a point in an infinite soil medium. The solution was obtained under the
13 assumption of elastic-plastic deformation of the soil with the Mohr-Coulomb-Tresca's-limit
14 yield criterion.

15 3. It is shown numerically that when solving the problem of cavity expansion in a soft
16 soil, it is necessary to take into account the formation of a plastic shock wave propagating
17 through the undisturbed portion of the soil.

18 4. The parametric analysis of the linearized rigid-plastic solution showed that it is a good
19 approximation of the dependence of pressure at the boundary of the cavity on the speed of its
20 expansion as applied to a wide class of soft soils.

21 5. On the basis of the proposed analytical solution, a method has been developed for
22 calculating the resistance force of a rigid body to penetrate into soft soil. The dependence of the
23 maximum value of the resistance force to the introduction of a rigid sphere into dry and water-
24 saturated sand, when the impact velocity varies in the range from 50 to 400 m/s, has been
25 obtained.

1 6. Comparison of the results for determining penetration resistance forces obtained
2 analytically, numerically and experimentally showed their qualitative and quantitative good
3 correspondence to each other. In this regard, when solving problems of penetration into soft
4 soils, a simple analytical solution can be successfully applied.

5

Preprint

The equation of motion in system (1) is written, neglecting the convective components of the time derivative of velocity:

$$\frac{\partial \sigma_r}{\partial r} + 2 \frac{(\sigma_r - \sigma_\theta)}{r} = -\rho \left(\frac{\partial v}{\partial t} \right), \quad v = \frac{\partial u}{\partial t}.$$

The radial and circumferential small strains in an elastic medium in conditions of spherical symmetry are defined in terms of displacements as $\varepsilon_r = \frac{\partial u}{\partial r}$, $\varepsilon_\theta = \frac{u}{r}$. The stress-strain

relation is described by Hooke's law: $-\sigma_r = \lambda \left(\frac{\partial u}{\partial r} + 2 \frac{u}{r} \right) + 2G \frac{\partial u}{\partial r} = (\lambda + 2G) \frac{\partial u}{\partial r} + 2\lambda \frac{u}{r}$,

$$\sigma_r - \sigma_\theta = 2G \left(\frac{u}{r} - \frac{\partial u}{\partial r} \right).$$

As before, stresses in compression are assumed to be positive.

The dynamic equation of an elastic medium in terms of displacements, in the case of spherical symmetry, is transformed into the following form:

$$\frac{\partial^2 u}{\partial r^2} + \frac{2}{r} \frac{\partial u}{\partial r} - \frac{2u}{r^2} = \frac{1}{c_e^2} \frac{\partial^2 u}{\partial t^2}, \quad (\text{A1})$$

where $c_e = \sqrt{(\lambda + 2G)/\rho_0} = \sqrt{(K + 4G/3)/\rho_0}$ is the velocity of propagation of the longitudinal wave front in an elastic medium.

Following [3], it is assumed that $\xi = r/ct$, $\tilde{u} = u/ct$ are, respectively a dimensionless coordinate and a dimensionless displacement, c is the plastic wave front velocity (i.e the velocity of the elastic-plastic interface), then the derivatives are transformed as follows, accounting for these changes of variables:

$$\frac{u}{r} = \frac{\tilde{u}}{\xi}, \quad \frac{\partial u}{\partial r} = \tilde{u}', \quad \frac{\partial^2 u}{\partial r^2} = \frac{1}{ct} \tilde{u}'' , \quad \frac{\partial^2 u}{\partial t^2} = \frac{c}{t} \xi^2 \tilde{u}''$$

where primes denote differentiation with respect to ξ .

The conditions on the boundary of the elastic deformation region are then considered. On the boundary with the unperturbed region, the displacement is equal to zero. On the elastic-

1 plastic interface $\xi = 1$ the condition of plastic yield $(\sigma_r - \sigma_\theta)|_{\xi=1} = f_2(\theta)$ holds, as well as
 2 Hooke's law: $\sigma_r - \sigma_\theta = 2G\left(\frac{u}{r} - \frac{\partial u}{\partial r}\right)$, whence, due to the continuity of the stress components, one
 3 has: $\left(\frac{u}{r} - \frac{\partial u}{\partial r}\right) = \frac{f_2(\theta)}{2G}$, $\theta = -\left(\frac{\partial u}{\partial r} + 2\frac{u}{r}\right)$. Transformation of the derivatives and substitution into
 4 equation (A1) and boundary conditions yield the following boundary-value problem for a
 5 second-order ordinary differential equation in terms of the dimensionless displacement:

$$6 \quad (1 - \alpha^2 \xi^2) \tilde{u}'' + \frac{2\tilde{u}'}{\xi} - \frac{2\tilde{u}}{\xi^2} = 0, \quad \alpha = c/c_e, \quad \tilde{u}(\xi = 1/\alpha) = 0 \quad (\text{A2})$$

$$7 \quad \left(\frac{\tilde{u}}{\xi} - \frac{\partial \tilde{u}}{\partial \xi}\right)\Bigg|_{\xi=1} = \frac{f_2(\theta)}{2G}, \quad \theta = -\left(\frac{\partial \tilde{u}}{\partial \xi} + 2\frac{\tilde{u}}{\xi}\right)\Bigg|_{\xi=1}.$$

8 To find a general solution to the differential equation, several transformations are done.
 9 Substituting $z = \alpha\xi$, one obtains the following equation:

$$10 \quad (1 - z^2) \frac{d^2 \tilde{u}}{dz^2} + \frac{2}{z} \frac{d\tilde{u}}{dz} - \frac{2\tilde{u}}{z^2} = 0.$$

11 Substitutions $\tilde{u} = z\varphi$, $F = d\varphi/dz$ yield a first-order equation for $F(z)$:

$$12 \quad z(1 - z^2)F' + 2(2 - z^2)F = 0 \quad \text{or} \quad \frac{dF}{F} = -\frac{2(2 - z^2)}{z(1 - z^2)} dz, \quad \text{a general solution for which is function}$$

13 $F(z) = \frac{A}{z^2} - \frac{A}{z^4}$ depending on an arbitrary constant A . Then the series of transformations:

$$14 \quad \frac{d\varphi}{dz} = \frac{A}{z^2} - \frac{A}{z^4}, \quad \varphi(z) = \frac{A}{3z^3} - \frac{A}{z} + B, \quad \tilde{u} = z\varphi: \quad \tilde{u} = \frac{A}{3z^2} - A + Bz, \quad z = \alpha\xi, \quad \text{result in the following}$$

15 expression for the dimensionless displacement: $\tilde{u} = A\left(\frac{1}{3\alpha^2\xi^2} - 1\right) + B\alpha\xi$, where B is another
 16 integration constant.

17 To define constants A , B , the boundary conditions in problem (A2) are used. From the
 18 first boundary condition it follows that $B = 2A/3$, thus,

$$19 \quad \tilde{u} = A\left(\frac{1}{3\alpha^2\xi^2} + \frac{2}{3}\alpha\xi - 1\right) = A\frac{(1 - \alpha\xi)^2(1 + 2\alpha\xi)}{3\alpha^2\xi^2} \quad (\text{A3})$$

1 Now by an expression for determining the dimensionless velocity

$$2 \quad U = \tilde{u} - \xi \frac{d\tilde{u}}{d\xi}, \quad U(\xi) = A \left(\frac{1 - \alpha^2 \xi^2}{\alpha^2 \xi^2} \right), \quad (\text{A4})$$

3 the radial component of the stress tensor and the volumetric strain will be derived:

$$4 \quad \sigma_r(\xi) = 2A \frac{(1 - \alpha\xi)}{\alpha^2 \xi^3} \left(K \alpha^2 \xi^2 + \frac{2G}{3} (1 + \alpha\xi) \right) \quad (\text{A5})$$

$$5 \quad \theta = - \left(\frac{\partial \tilde{u}}{\partial \xi} + 2 \frac{\tilde{u}}{\xi} \right) = 2A \left(\frac{1 - \alpha\xi}{\xi} \right). \quad (\text{A6})$$

6 Employing now equality (A6), equations for both dimensionless velocity (A4) and stress
7 (A5) can be transformed into the following form:

$$8 \quad U(\xi) = \left(\frac{1 + \alpha\xi}{2\alpha^2 \xi} \right) \theta(\xi), \quad \sigma_r(\xi) = \left(K + \frac{2G}{3} \frac{(1 + \alpha\xi)}{\alpha^2 \xi^2} \right) \theta(\xi). \quad (\text{A7})$$

9 To define the integration constant A , the second boundary condition of the boundary-
10 value problem (A2) is considered. Strain difference for $\xi = 1$ is defined as
11 $(\tilde{u}/\xi - \partial\tilde{u}/\partial\xi)_{\xi=1} = A(\alpha^{-2} - 1)$. Thus, constant A is determined by solving the equation

$$12 \quad 2GA \left((1 - \alpha^2) / \alpha^2 \right) = f_2(2A(1 - \alpha)).$$

13 This problem was solved earlier in [3], using Tresca's yield condition. Consider Mohr-
14 Coulomb-Tresca's plasticity condition; in this case function f_2 becomes:

$$15 \quad f_2 \equiv \begin{cases} \tau_0 + kK\theta, & 0 < \theta \leq \theta_M, \\ \tau_M, & \theta \geq \theta_M \end{cases}, \quad \theta_M = \frac{\tau_M - \tau_0}{kK}.$$

16 So, for $\xi = 1$ one has:

$$17 \quad \theta = \begin{cases} \tau_0 / (G(\alpha) - kK), & G(\alpha) > G^*, \\ \tau_M / G(\alpha), & G(\alpha) \leq G^* \end{cases} \quad (\text{A8})$$

18 where: $G(\alpha) = (1 + \alpha)G / \alpha^2$, $G^* = \tau_M kK / (\tau_M - \tau_0) = \tau_M / \theta_M$.

19 Expressions (A7), (A8) for $\xi = 1$ will define the boundary conditions for the problem from
20 Section 3.2. as a function of the value of α :

$$1 \quad U^e = U(\xi=1) = \frac{(1+\alpha)}{2\alpha^2} \theta, \quad S^e = S(\xi=1) = (\tilde{K} + 2/3\tilde{G})\theta, \quad (\text{A9})$$

2 where θ is defined by expression (A6), $\tilde{K} = K/r_0c^2$, $\tilde{G} = G(\alpha)/r_0c^2$.

3 In the limiting case, for $\alpha = 1$, which corresponds to equality $c = c_e$, equations (A9) take

4 the form defined by Hugoniot's relations at the jump: $U^e = \theta$,

$$5 \quad S^e = (\tilde{K} + 4/3\tilde{G})\theta = \frac{c_e^2}{c_2} \theta = \alpha^2 \theta = \theta.$$

6

Preprint

1 **Funding:** the investigations were supported by the grant of the Government of the Russian
2 Federation (contract No.14.Y26.31.0031).

3

4 **Conflict of Interest:** The authors declare that they have no conflict of interest.

5

6

7 **References**

8

- 9 [1] Forrestal MJ, Longcope DB. Closed-form solution for forces on conical-nosed penetrators
10 into geological targets with constant shear strength. *Mechanics of Materials* 1982; **1**(4): 285-
11 295.
- 12 [2] Forrestal MJ, Norwood FR, Longcope DB. Penetration into targets described by locked
13 hydrostats and shear strength. *Int. J. Solids Structures* 1981; **17**(9): 915-924.
- 14 [3] Forrestal MJ, Luk VK. Penetration into soil targets. *Int. J. Impact. Eng.* 1992; **12**(3): 427-
15 444.
- 16 [4] Forrestal MJ, Luk VK. Dynamic spherical cavity-expansion in a compressible elastic-plastic
17 solid. *Trans. ASME. J. Appl. Mech.* 1988; **55**(2): 275-279.
- 18 [5] Durban D, Masri R. Dynamic spherical cavity expansion in a pressure sensitive elastoplastic
19 medium. *Int. J. Solids Structures* 2004; **41**(20): 5697-5716.
- 20 [6] Meng C, Tan Q, Jiang Z, Song D, Liu F. Approximate solutions of finite dynamic spherical
21 cavity-expansion models for penetration into elastically confined concrete targets. *Int. J.*
22 *Impact Eng.* 2018; **114**: 182–193.
- 23 [7] Cleja-Tigoiu S, Cazacu O, Tigoiu V. Dynamic expansion of spherical cavity within a rate-
24 dependent compressible porous material. *Int. J. Plasticity* 2008; **24** (5): 775-803.

- 1 [8] Feng J, Li WB, Wang XM, Song ML, Ren HQ, Li WB. Dynamic spherical cavity expansion
2 analysis of rate-dependent concrete material with scale effect. *Int. J. Impact Eng.* 2015; **84**:
3 24–37.
- 4 [9] Rosenberg Z, Dekel E. A numerical study of the cavity expansion process and its application
5 to long-rod penetration mechanics. *Int. J. Impact Eng.* 2008; **35**(3): 147-154.
- 6 [10] Rosenberg Z, Dekel E. Analytical solution of the spherical cavity expansion process. *Int.*
7 *J. Impact Eng.* 2009; **36** (2): 193-198.
- 8 [11] Masri R, Durban D. Deep penetration analysis with dynamic cylindrical cavitation fields.
9 *Int. J. Impact Eng.* 2009; **36**(6): 830–841.
- 10 [12] Masri R, Durban D. Cylindrical cavity expansion in compressible Mises and Tresca
11 solids. *European J. Mechanics A/Solids* 2007; **26**(4): 712-727.
- 12 [13] Suzuki Y, Lehane BM. Analysis of CPT end resistance at variable penetration rates using
13 the spherical cavity expansion method in normally consolidated soils. *Computers and*
14 *Geotechnics* 2015; **69**: 141–152.
- 15 [14] Cheng Y, Yang H-W, Sun D. Cavity expansion in unsaturated soils of finite radial extent.
16 *Computers and Geotechnics* 2018; **102**: 216–228.
- 17 [15] Su D, Yang ZX. Drained analyses of cylindrical cavity expansion in sand incorporating a
18 bounding-surface model with state-dependent dilatancy. *Applied Mathematical Modelling*
19 2019; **68**: 1-20
- 20 [16] Shi C, Wang M, Li J, Li M. A model of depth calculation for projectile penetration into
21 dry sand and comparison with experiments. *Int. J. Impact Eng.* 2014; **73**: 112-122.
- 22 [17] Shi C, Wang M, Zhang K, Cheng Y, Zhang X. Semi-analytical model for rigid and
23 erosive long rods penetration into sand with consideration of compressibility. *Int. J. Impact*
24 *Eng.* 2015; **83**: 1-10.
- 25 [18] Yu H-S. *Cavity Expansion Methods in Geomechanics*. Dordrecht: Kluwer, 2000.

- 1 [19] Ben-Dor G, Dubinsky A, Elperin T. Applied High-Speed Plate Penetration Dynamics.
2 Dordrecht: Springer, 2006.
- 3 [20] Ben-Dor G, Dubinsky A, Elperin T. Engineering models of high speed penetration into
4 geological shields. *Central European J. Eng.* 2014; **1**(4): 1–19.
- 5 [21] Omidvar M, Iskander M, Bless S. Response of granular media to rapid penetration. *Int. J.*
6 *Impact Eng.* 2014; **66**: 60–82.
- 7 [22] Omidvar M, Doreau-Malioche J, Bless S, Iskander M. Phenomenology of rapid projectile
8 penetration into granular soils. *Int. J. Impact Eng.* 2015; **85**: 146-160.
- 9 [23] Forrestal MJ, Tzou DY, Askari E, Longcope DB. Penetration into ductile metal targets
10 with rigid spherical-nose rods. *Int. J. Impact Eng.* 1995; **16**(5/6):699–710.
- 11 [24] Chen XW, Li QM. Deep penetration of a non-deformable projectile with different
12 geometrical characteristics. *Int. J. Impact Eng.* 2002; **27**(6): 619-637.
- 13 [25] Forrestal MJ, Warren TL. Penetration equations for ogive-nose rods into aluminum
14 targets. *Int. J. Impact Eng.* 2008; **35**(8): 727–730.
- 15 [26] Warren TL. The effect of target inertia on the penetration of aluminum targets by rigid
16 ogive-nosed projectiles. *Int. J. Impact Eng.* 2016; **91**: 6–13.
- 17 [27] Rosenberg Z, Dekel E. A comment on “The effect of target inertia on the penetration of
18 aluminum targets by rigid ogive-nosed long rods” by T.L. Warren *Int. J. Impact Eng.* 2016,
19 *Int. J. Impact Eng.* 2016; **93**: 231–233.
- 20 [28] Warren TL. Response to: A comment on “The effect of target inertia on the penetration
21 of aluminum targets by rigid ogive-nosed long rods” by T.L. Warren, *Int. J. Impact Eng.*
22 2016 by Z. Rosenberg and E. Dekel. *Int. J. Impact Eng.* 2016; **93**: 234–235.
- 23 [29] Kong XZ, Wu H, Fang Q, Peng Y. Rigid and eroding projectile penetration into concrete
24 targets based on an extended dynamic cavity expansion model. *Int. J. Impact Eng.* 2017;
25 **100**:13–22.

- 1 [30] Rosenberg Z, Kositski R, Dekel E. Comment on: “Rigid and eroding projectile
2 penetration into concrete targets based on an extended dynamic cavity expansion model” by
3 Kong *et al.* *Int. J. Impact Eng.* (2017), *Int. J. Impact Eng.* 2017; **104**: A1-A3.
- 4 [31] Kong XZ, Wu H, Fang Q, Peng Y. Response to: Comment on “Rigid and eroding
5 projectile penetration into concrete targets based on an extended dynamic cavity expansion
6 model” by Kong *et al.* *Int. J. Impact Eng.* 2017 by Z. Rosenberg *et al.* *Int. J. Impact Eng.*
7 2017; **104**: 150-153.
- 8 [32] Warren TL, Hanchak SJ, Poormon KL. Penetration of limestone targets by ogive-nosed
9 VAR 4340 steel projectiles at oblique angles: experiments and simulations. *Int. J. Impact*
10 *Eng.* 2004; **30**(10): 1307-1331.
- 11 [33] Warren TL. Simulations of the penetration of limestone targets by ogive-nose 4340 steel
12 projectiles. *Int. J. Impact Eng* 2002; **27**(5): 475–496.
- 13 [34] Li QM, Flores-Johnson EA. Hard projectile penetration and trajectory stability. *Int. J.*
14 *Impact Eng.* 2011; **38**(10): 815–823.
- 15 [35] Sun Q, Sun Y, Liu Y, Li R, Zhao Y. Numerical analysis of the trajectory stability and
16 penetration ability of different lateral-abnormal projectiles for non-normal penetration into
17 soil based on Modified Integrated Force Law method. *Int. J. Impact Eng.* 2017; **103**: 159-
18 168.
- 19 [36] Kotov VL, Balandin VV, Bragov AM, Linnik EYu, Balandin VV. Using a local-
20 interaction model to determine the resistance to penetration of projectiles into sandy soil.
21 *Journal of Applied Mechanics and Technical Physics* 2013; **54**(4): 612–621.
- 22 [37] Bazhenov VG, Balandin VV, Grigoryan SS, Kotov VL. Analysis of models for
23 calculating the motion of solids of revolution of minimum resistance in soil media. *Journal*
24 *of Applied Mathematics and Mechanics.* 2014; **78**(1): 65-76.

- 1 [38] Balandin VIV, BalandinVIVI, Bragov AM, Kotov VL. Experimental study of the
2 dynamics of penetration of a solid body into a soil medium. *Technical Physics* 2016; **61**(6):
3 860–868.
- 4 [39] Kotov VL, Balandin VV, Bragov AM, and Balandin VIVI. Investigation of dynamic
5 resistance to the shear of water-saturated sand according to the results of the
6 InverseExperiment Technique. *Technical Physics Letters* 2017; **43**(9): 808–810.
- 7 [40] Bragov AM, Balandin VIV, Kotov VL, Balandin VIVI. Investigation of the dynamic
8 properties of water-saturated sand by the results of inverted experiments. *Technical Physics*
9 2018; **63**(4): 530–539.
- 10 [41] Bragov AM, Balandin VV, Igumnov LA, Kotov VL, Krushka L, Lomunov AK. Impact
11 and penetration of cylindrical bodies into dry and water-saturated sand. *Int. J. Impact Eng.*
12 2018; **122**: 197-208.
- 13 [42] Lyakhov GM. Shock waves in soil and water sand dilution. *Zh. Prikl. Mekh. Tekhn. Fiz.*
14 1961; **2**(1): 38–46. [English translation in: *J. Appl. Mech. Tech. Phys.*].
- 15 [43] Lyakhov GM. Experimental study of blast waves in clayey soil. *Zh. Prikl. Mekh. Tekhn.*
16 *Fiz.* 1961; **2**(2): 123–126. [English translation in: *J. Appl. Mech. Tech. Phys.*].
- 17 [44] Rykov GV. Experimental study of stress field in an explosion in sandy soil. *Zh. Prikl.*
18 *Mekh. Tekhn. Fiz.* 1964; **5**(1): 85–89. [English translation in: *J. Appl. Mech. Tech. Phys.*].
- 19 [45] Lagunov VA, Stepanov VA. Measurements of the dynamic compressibility of sand under
20 high pressures . *Zh. Prikl. Mekh. Tekhn. Fiz.* 1963; **4**(1): 88–96. [English translation in: *J.*
21 *Appl. Mech. Tech. Phys.*].
- 22 [46] Arlery M, Gardou M, Fleureau JM, Mariotti C. Dynamic behaviour of dry and water-
23 saturated sand under planar shock conditions. *Int. J. Impact Eng.* 2010; **37**(1): 1–10.
- 24 [47] Kinslow R. *High-Velocity Impact Phenomena*. New York and London: Academic Press,
25 1970.

- 1 [48] Bragov AM, Lomunov AK, Sergeichev IV, Tsembelis K, Proud WG. Determination of
2 physicommechanical properties of soft soils from medium to high strain rates. *Int. J. Impact*
3 *Eng.* 2008; **35**(9): 967-976.
- 4 [49] Bazhenov VG, Bragov AM, Kotov VL, Kochetkov AV. An investigation of the impact
5 and penetration of solids of revolution into soft earth. *J. Appl. Math. Mech.* 2003; **67**(4):
6 611–620.
- 7 [50] Bazhenov VG, Kotov VL, Kochetkov AV, Krylov SV, Feldgun VR. On wave processes
8 in soil subjected to a surface charge explosion. *Mechanics of Solids* 2001; **36**(2): 62-68.
- 9 [51] Linnik EYu, Kotov VL, Tarasova AA, Gonik EG. The solution of the problem of the
10 expansion of a spherical cavity in a soil medium assuming incompressibility beyond the
11 shock front. *Problems of Strength and Plasticity* 2012; **74**: 49-58. [in Russian].
- 12 [52] Allen WA, Mayfield EB, Morrison HL. Dynamics of a projectile penetrating sand. *J.*
13 *Appl. Physics* 1957; **28**(3): 370-376.